



Stoichiometry and environmental change drive dynamical complexity and unpredictable switches in an intraguild predation model

Juping Ji¹ · Russell Milne¹ · Hao Wang¹

Received: 4 January 2022 / Revised: 17 November 2022 / Accepted: 2 January 2023

© The Author(s), under exclusive licence to Springer-Verlag GmbH Germany, part of Springer Nature 2023

Abstract

We incorporate stoichiometry (the balance of key elements) into an intraguild predation (IGP) model. Theoretical and numerical results show that our system exhibits complex dynamics, including chaos and multiple types of both bifurcations and bistability. Types of bifurcation present include saddle-node, Hopf, and transcritical bifurcations, and types of bistability present include node-node, node-cycle, and cycle-cycle bistability; cycle-cycle bistability has never been observed in IGP ordinary differential equation models. Stoichiometry can stabilize or destabilize the system via the disappearance or appearance of chaos. The species represented in the model can coexist for moderate levels of light intensity and nutrient availability. When the amount of light or nutrients present is extremely high or low, coexistence of the species becomes impossible, potentially harming biodiversity. Interestingly, stoichiometry can facilitate the re-emergence of severely endangered species as light intensity increases. In a temporally changing environment, the system can jump between different unstable states following changes in light intensity, with the trajectory followed depending strongly on initial conditions.

Keywords Stoichiometry · Intraguild predation model · Light intensity · Nutrient availability · Environmental change

Mathematics Subject Classification 34C23 · 34D20 · 37G15 · 92B05

✉ Hao Wang
hao8@ualberta.ca

¹ Department of Mathematical and Statistical Sciences, University of Alberta, Edmonton, AB T6G 2R3, Canada

1 Introduction

Within the field of ecology, it has long been known that organisms require the intake of nutrients in specific ratios in order to grow (Redfield 1958), with the study of these ratios and how they affect other ecological processes being referred to as stoichiometry. Carbon (C), nitrogen (N) and phosphorus (P) are three of the most common nutrients in any organism, and the ability of organisms to maintain a balance of these three has therefore been heavily focused on Jeyasingh et al. (2017), Redfield (1958), although many other nutrients such as iron (Fe) and silicon (Si) can also serve as limiting factors for organismal growth (Moore et al. 2002). These nutrient ratios are not constant across species: for instance, a review of nutrient density in aquatic primary producers found phytoplankton to have lower carbon:nitrogen and carbon:phosphorus ratios than algae or seagrass (Duarte 1992). Even within a species, nutrient ratios may change over time as a given organism develops (Pilati and Vanni 2007). These differences occur because different organisms perform different vital biological processes, and thus necessarily have different nutrient requirements.

A corollary of this is that the nutrients that a predator species consumes by eating its prey may not be available in the predator species's desired ratio (Moe et al. 2005). This means that stoichiometry can greatly influence the stability of food webs, and hence studying within-species nutrient balances and between-species energy and nutrient flows can help to indicate an ecosystem's health. Similarly, stoichiometry can be used to predict the susceptibility of an ecosystem to invasion by species whose nutrient needs are a closer match for local nutrient ratios than those of the native species (Andersen et al. 2004), which is a particular concern in aquatic environments affected by nutrient loading (Glibert 2012). Because of this, much research attention in biology has been paid to ecological stoichiometry (e.g. Andersen 1997; Andersen et al. 2004; Andersen and Hessen 1991; Elser et al. 1996; Sterner and Elser 2002).

In addition to field biology, there has also been widespread interest in ecological stoichiometry within the field of mathematical modelling, with many researchers incorporating stoichiometry into ecological models (e.g. Heggerud et al. 2020; Kuang et al. 2004; Li and Wang 2010; Lin et al. 2012; Loladze et al. 2000, 2004; Wang et al. 2007). For instance, Loladze et al. (2000) proposed a stoichiometric producer-grazer model (LKE model), with the nutrients represented in the model being carbon and phosphorus. It was assumed that the producer would be able to uptake carbon freely from the atmosphere (in the form of carbon dioxide), with its ability to do so being governed by the availability of light for photosynthesis, so light intensity was used as a proxy for carbon availability. In contrast, the producer was assumed to uptake phosphorus from dead or excreted matter if it was available, up to the point where it would reach its optimal carbon:phosphorus ratio. The fact that the two nutrients were obtained using different mechanisms, but each one was potentially growth-limiting, led to rich dynamics. For instance, in the LKE model, light energy enrichment can either destabilize or stabilize the system, and can also lead to the eventual extinction of the grazer. On the contrary, phosphorus enrichment can destabilize the system but not stabilize it, and it cannot cause the grazer to go extinct. Further results from the LKE model also replicated Rosenzweig's paradox of enrichment, within a limited range of light and nutrient availability.

Later, Li et al. (2011) analyzed the effects of including different Holling-type functional responses (Types I and II) on the dynamics of the LKE stoichiometric producer-grazer model. As the Holling Type II functional response caused the model to become highly complex, Li et al. specifically focused on the effects of changing the light intensity in this case. When varying the producer's carrying capacity, which was measured in terms of the producer's carbon biomass and hence determined by light availability, bistability as well as many different bifurcation types were visible. Further analysis was performed by Xie et al. (2018), who determined the behaviour of the LKE model when other environmental conditions besides light intensity were taken to vary. Their work concluded that increasing nutrient availability causes the system to have richer and more complicated dynamics. This included four distinct types of bistability: the bistability between an internal equilibrium and a limit cycle found in Li et al. (2011) as well as three newly found ones.

Based on the LKE model, Peace (2015) proposed a stoichiometric aquatic food chain model and explored effects of nutrient enrichment, light availability, and food chain length. This stoichiometric food chain model contained three species, namely a producer, a consumer, and a predator. In the context of an aquatic environment, these can be considered to be phytoplankton, zooplankton, and fish, respectively. In the model, it was assumed that the P:C (phosphorus:carbon) ratio of the producer could vary, but would never fall below a certain value. In contrast, the consumer and predator were assumed to have constant P:C ratios. The consumer-producer and predator-consumer trophic interactions were both assumed to be Holling Type II functional responses. Adding the predator species into the food chain led to the result that the efficiency of energy transfer in predator-prey interactions is lower in tritrophic food chain compared to food chains with only two levels by an order of magnitude. This underlines the importance of ecological stoichiometry in maintaining trophic connections, as it means that predator species whose nutrient needs most closely match those of their prey (and therefore have similar nutrient ratios) will have a significant competitive advantage.

In addition to trophic models, further work on incorporating ecological stoichiometry into models of inter-specific competition was done by Rong et al. (2020). They studied a stoichiometric competition model containing two competing herbivores feeding on one herbaceous plant, where the plant in question was divided into an above-ground component (which can perform photosynthesis but can also be eaten by the herbivores) and a below-ground component (for which neither photosynthesis nor predation happen). In this model, it was found that intermediate levels of both light intensity and nitrogen availability resulted in coexistence of all three species. However, increasing either nitrogen availability or light intensity resulted in one of the two herbivores outcompeting the other; which herbivore was more competitive directly depended on the optimal N:C ratios for each species. Additional findings included the fact that extremely high nitrogen levels could cause the herbaceous plant to go extinct due to high levels of predation, in a variation on the paradox of enrichment.

Besides predation and competition, another widespread fundamental relationship in ecological communities is intraguild predation (IGP). IGP involves two or more competing predator species that have the same prey, where the predator species can also kill and eat each other. Examples of this have been found across many biological

taxa. For instance, coyotes, bobcats and kit foxes in western North America all have a primary diet of small mammals such as rodents, but coyotes (the largest of the three species) also eat bobcats and kit foxes (Fedriani et al. 2000; Lonsinger et al. 2017), and bobcats eat kit foxes on occasion as well (Fedriani et al. 2000). IGP is also important in the context of invasive species, as an introduced species can gain a competitive advantage over a local species occupying the same niche by preying on the local species's juveniles. This behaviour has been observed among different species of anole lizard (Gerber and Echternacht 2000; Ji et al. 2022a), as well as lionfish and groupers in the Caribbean Sea (Leung et al. 2015; Mumby et al. 2011). Holt and Polis (1997) proposed a general modeling framework to describe the species interactions that characterize IGP:

$$\begin{cases} \frac{dx}{dt} = rx \left(1 - \frac{x}{K}\right) - f(x)y - g(x)z, \\ \frac{dy}{dt} = e_1 f(x)y - h(y)z - d_1 y, \\ \frac{dz}{dt} = e_2 g(x)z + e_3 h(y)z - d_2 z. \end{cases} \quad (1.1)$$

Many IGP models based on this framework have been proposed and extensively studied (e.g. Han et al. 2018; Hsu et al. 2015; Ji et al. 2022b; Ji and Wang 2022; Sen et al. 2018; Shu et al. 2015). It is well known that nonstoichiometric IGP models can have very rich and complex dynamics, like chaos and multistability. However, existing IGP models typically only consider organismal growth as a function of food quantity, in the form of density-dependent growth rates. In reality, the growth rate of a producer is based on multiple factors, with two of the most biochemically important being the amount of energy that they can obtain via photosynthesis and the amount of nutrients that they can uptake from their surroundings. In turn, the growth of consumers also depends on acquiring nutrients by eating other organisms, and hence availability of both nutrients and light to producers has a strong indirect effect on population levels of species elsewhere in a food web. Because stoichiometric population models can properly describe how light and nutrients affect population reproduction, and intraguild predation is common in many different ecosystems worldwide, it is therefore important to evaluate how incorporating ecological stoichiometry into an IGP model affects population stability of the model species.

In most cases, ecological models are studied under the assumptions that environmental conditions are constant. However, the conditions that drive population growth, such as the availability of light and nutrients, may undergo both long-term and short-term change. For instance, increases in atmospheric carbon dioxide are associated with greater rates of photosynthesis in plants, and hence greater carbon uptake (Dusenge et al. 2019). Likewise, other external factors such as temperature can also affect photosynthetic rates (e.g. Crous et al. 2013; Robakowski et al. 2012), meaning that the balance of nutrients within a producer species may change even if the amount of each nutrient available remains constant. It has recently been shown that the rate of environmental change has an impact on the behavior of a predator–prey system: Arumugam et al. (2021) studied the dynamics of predator–prey metacommunity models in a varying environment. Their results revealed that in a changing environment, the composition of a predator–prey system can spend significant amounts of time near equilibria that are unstable under the assumptions of static environmental conditions.

This finding in a relatively simple model (a two-patch metacommunity without stoichiometric considerations) means that other dynamics like it are possible in a more complex one.

The rest of this paper is organized as follows. In Sect. 2, we propose a stoichiometric IGP model, as well as a corresponding model that features environmental change. In Sect. 3, well-posedness and dynamics of the system are studied. In Sect. 4, we carry out some numerical simulations to explore the dynamics for different levels of light intensity and nutrient availability. In Sect. 5, the effects of environmental change on the model dynamics are discussed. We conclude our results briefly in the last section.

2 Model formulation

In this work, we consider the effects of two essential elements, carbon (C) and phosphorus (P), and assume that all other elements are abundant in the environment. The ratio of these two essential chemical elements (i.e. phosphorus to carbon) represents producer quality. This is because it is assumed that there is a fixed total amount of P in the environment, while carbon uptake by the producer is instead restricted by its ability to undergo photosynthesis; if light is abundant, there will be fewer limits on C compared to P.

Existing works mainly explore the competition or predation in ecological stoichiometric models, with comparatively little work on stoichiometric IGP models. Our intent is to incorporate stoichiometry into an IGP model to explore how altering the availability of nutrients and light changes the model dynamics. Bearing this goal in mind, in this paper, we propose a stoichiometric IGP model

$$\begin{cases} \frac{dx}{dt} = rx \left(1 - \frac{x}{\min\{K, (P - \theta_1 y - \theta_2 z)/q\}} \right) - f(x)y - g(x)z, \\ \frac{dy}{dt} = e_1(x, y, z) f(x)y - h(y)z - d_1 y, \\ \frac{dz}{dt} = e_2(x, y, z) g(x)z + e_3(y, z) h(y)z - d_2 z, \end{cases} \quad (2.1)$$

where

$$\begin{aligned} e_1(x, y, z) &= \min \left\{ e_1, \frac{(P - \theta_1 y - \theta_2 z)/x}{\theta_1} \right\}, \\ e_2(x, y, z) &= \min \left\{ e_2, \frac{(P - \theta_1 y - \theta_2 z)/x}{\theta_2} \right\}, \\ e_3(y, z) &= \min \left\{ e_3, \frac{\theta_1}{\theta_2} \right\}. \end{aligned}$$

Here x , y and z denote the biomass of the plant, herbivore, and omnivore, respectively, measured in terms of C (carbon). The minimum function $\min\{K, (P - \theta_1 y - \theta_2 z)/q\}$ describes the plant carrying capacity. In this function, K is the carrying capacity determined by light availability (if phosphorus is plentiful), while $(P - \theta_1 y - \theta_2 z)/q$ is the carrying capacity determined by phosphorus availability, where θ_1 is the constant P:C ratio of the herbivore and θ_2 is the constant P:C ratio of the omnivore. The

growth efficiency of the herbivore $e_1(x, y, z)$ depends on both energy and nutrients. When $(P - \theta_1 y - \theta_2 z)/e_1 x > \theta_1$, the growth of the herbivore is limited by carbon and $e_1(x, y, z) = e_1$. When $(P - \theta_1 y - \theta_2 z)/e_1 x < \theta_1$, the growth of the herbivore is instead limited by phosphorus and $e_1(x, y, z) = (P - \theta_1 y - \theta_2 z)/x\theta_1$. Similarly, we use a minimum function $e_2(x, y, z) = \min \left\{ e_2, \frac{(P - \theta_1 y - \theta_2 z)/x}{\theta_2} \right\}$ to denote the growth efficiency of the omnivore from consuming the plant. Likewise, $e_3(y, z) = \min \left\{ e_3, \frac{\theta_1}{\theta_2} \right\}$ describes the growth efficiency of the omnivore from consuming the herbivore. If $\theta_1 > e_3\theta_2$, then the nutrients contained in the herbivore are sufficient for the omnivore population to grow at its fastest possible rate. However, if $\theta_1 < e_3\theta_2$, then the omnivore will not be able to fully utilize the C that it obtains by consuming the herbivore.

The functional responses $f(x)$, $g(x)$ and $h(y)$ describe the rates at which the herbivore ingests the plant, the omnivore ingests the plant, and the omnivore ingests the herbivore, respectively. If $g(x) = 0$, System (2.1) reduces to a stoichiometric food chain model. The frequently used functional responses are the classical Holling type I, II, and III functional responses (Holling 1959a, b, 1966). In this paper, $f(x)$, $g(x)$ and $h(y)$ are taken to be Monod functions (Holling type II functions):

$$f(x) = \frac{c_1 x}{a_1 + x}, \quad g(x) = \frac{c_2 x}{a_2 + x}, \quad h(y) = \frac{c_3 y}{a_3 + y}.$$

The following three assumptions are made in this model:

A1: The total mass of phosphorus in the entire system is fixed, i.e., the system is closed for phosphorus with a total of $P \text{ mg P L}^{-1}$.

A2: The plant’s P:C ratio varies, but never falls below a minimum $q \frac{\text{mg P}}{\text{mg C}}$; the herbivore and the omnivore maintain a constant P:C, θ_1 and $\theta_2 \frac{\text{mg P}}{\text{mg C}}$, respectively.

A3: All phosphorus in the system is divided into three pools: phosphorus in the herbivore, in the omnivore and in the plant.

A schematic diagram for System (2.1) is presented in Fig. 1. The description of the parameters of System (2.1) is specified in Table 1.

In this work, we intend to discuss the effect of environmental change on the system dynamics. This change is reflected in changes in the plant’s carrying capacity. Here, we assume the environment changes linearly, that is carrying capacity (K) of the plant increases or decreases linearly. After this change, we get the following system:

$$\begin{cases} \frac{dx}{dt} = rx \left(1 - \frac{x}{\min\{K, (P - \theta_1 y - \theta_2 z)/q\}} \right) - f(x)y - g(x)z, \\ \frac{dy}{dt} = e_1(x, y, z)f(x)y - h(y)z - d_1 y, \\ \frac{dz}{dt} = e_2(x, y, z)g(x)z + e_3(y, z)h(y)z - d_2 z, \\ \frac{dK}{dt} = \mu, \end{cases} \tag{2.2}$$

where μ is the rate of environmental change.

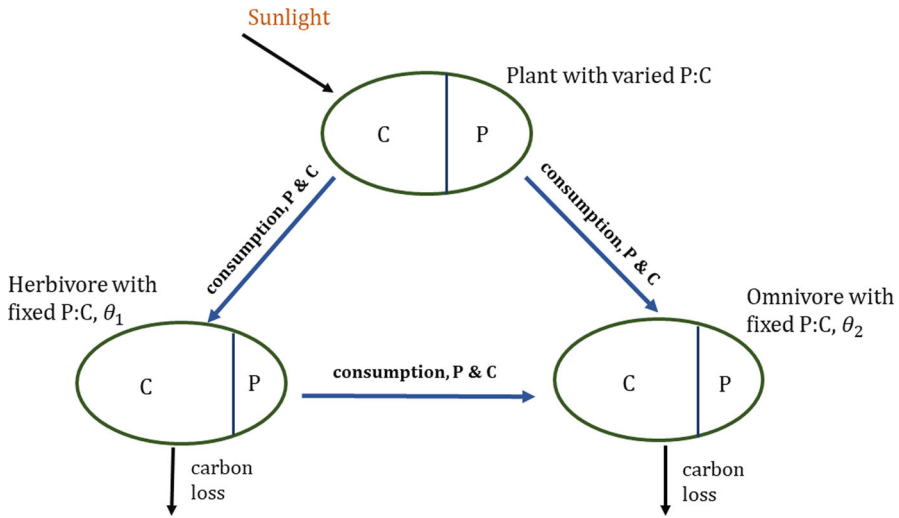


Fig. 1 A schematic diagram describing the interactions among species in the model

3 Qualitative analysis

In this section, we investigate the dynamics of System (2.1). For simplicity, let

$$\begin{aligned}
 u &= \frac{x}{a_1}, \quad v = \frac{c_1 y}{r a_1}, \quad w = \frac{c_2 z}{r a_1}, \quad \tau = r t, \quad k = \frac{K}{a_1}, \quad p = \frac{P}{q a_1}, \\
 \gamma_1 &= \frac{c_1 e_1}{r}, \quad \gamma_2 = \frac{c_2 e_2}{r}, \quad \gamma_3 = \frac{c_3 e_3}{r}, \quad \alpha_1 = \frac{a_2}{a_1}, \quad \alpha_2 = \frac{c_1 a_3}{r a_1}, \quad \beta_1 = \frac{r \theta_1}{q c_1}, \\
 \beta_2 &= \frac{r \theta_2}{q c_2}, \quad \delta_1 = \frac{d_1}{r}, \quad \delta_2 = \frac{d_2}{r}, \quad \varepsilon = \frac{c_1 c_3}{r c_2}.
 \end{aligned}$$

We replace τ by t whenever no confusion arises, and obtain the dimensionless system

$$\begin{cases}
 \frac{du}{dt} = u \left(1 - \frac{u}{\min\{k, p - \beta_1 v - \beta_2 w\}} \right) - \frac{uv}{1+u} - \frac{uw}{\alpha_1 + u} := uF(u, v, w), \\
 \frac{dv}{dt} = \min \left\{ \gamma_1, \frac{p - \beta_1 v - \beta_2 w}{\beta_1 u} \right\} \frac{uv}{1+u} - \frac{\varepsilon v w}{\alpha_2 + v} - \delta_1 v := vG(u, v, w), \\
 \frac{dw}{dt} = \min \left\{ \gamma_2, \frac{p - \beta_1 v - \beta_2 w}{\beta_2 u} \right\} \frac{uw}{\alpha_1 + u} + \min \left\{ \gamma_3, \frac{\varepsilon \beta_1}{\beta_2} \right\} \frac{v w}{\alpha_2 + v} - \delta_2 w := wH(u, v, w).
 \end{cases} \tag{3.1}$$

Here,

$$\begin{aligned}
 F(u, v, w) &= 1 - \frac{u}{\min\{k, p - \beta_1 v - \beta_2 w\}} - \frac{v}{1+u} - \frac{w}{\alpha_1 + u} \\
 &= \begin{cases} 1 - \frac{u}{k} - \frac{v}{1+u} - \frac{w}{\alpha_1 + u}, & k \leq p - \beta_1 v - \beta_2 w; \\ 1 - \frac{u}{p - \beta_1 v - \beta_2 w} - \frac{v}{1+u} - \frac{w}{\alpha_1 + u}, & k > p - \beta_1 v - \beta_2 w. \end{cases}
 \end{aligned}$$

Table 1 Parameters in System (2.1)

Parameter	Description	Unit
r	Maximal growth rate of plant	1/day
K	Plant carrying capacity limited by light	mgC/L
P	Total phosphorus	mgP/L
θ_1	Herbivore constant P:C	mgP/mgC
θ_2	Omnivore constant P:C	mgP/mgC
q	Plant minimal P:C	mgP/mgC
a_1	Half saturation of the herbivore ingestion response to plant	mgC/L
a_2	Half saturation of the omnivore ingestion response to plant	mgC/L
a_3	Half saturation of the omnivore ingestion response to herbivore	mgC/L
c_1	Maximal ingestion rate of the herbivore on plant	1/day
c_2	Maximum ingestion rate of the omnivore on plant	1/day
c_3	Maximum ingestion rate of the omnivore on herbivore	1/day
e_1	Maximal herbivore production efficiency from consuming plant	unitless
e_2	Maximal omnivore production efficiency from consuming plant	unitless
e_3	Maximal omnivore production efficiency from consuming herbivore	unitless
d_1	Herbivore loss rate	1/day
d_2	Omnivore loss rate	1/day

$$\begin{aligned}
 G(u, v, w) &= \min \left\{ \gamma_1, \frac{p - \beta_1 v - \beta_2 w}{\beta_1 u} \right\} \frac{u}{1 + u} - \frac{\varepsilon w}{\alpha_2 + v} - \delta_1 \\
 &= \begin{cases} \frac{\gamma_1 u}{1 + u} - \frac{\varepsilon w}{\alpha_2 + v} - \delta_1, & \gamma_1 \beta_1 u \leq p - \beta_1 v - \beta_2 w; \\ \frac{p - \beta_1 v - \beta_2 w}{\beta_1 (1 + u)} - \frac{\varepsilon w}{\alpha_2 + v} - \delta_1, & \gamma_1 \beta_1 u > p - \beta_1 v - \beta_2 w. \end{cases}
 \end{aligned}$$

$$H(u, v, w) = \min \left\{ \gamma_2, \frac{p - \beta_1 v - \beta_2 w}{\beta_2 u} \right\} \frac{u}{\alpha_1 + u} + \min \left\{ \gamma_3, \frac{\varepsilon \beta_1}{\beta_2} \right\} \frac{v}{\alpha_2 + v} - \delta_2$$

$$= \left\{ \begin{array}{ll} \frac{\gamma_2 u}{\alpha_1 + u} + \frac{\gamma_3 v}{\alpha_2 + v} - \delta_2, & \gamma_2 \beta_2 u \leq p - \beta_1 v - \beta_2 w, \\ & \gamma_3 \beta_2 \leq \varepsilon \beta_1; \\ \frac{p - \beta_1 v - \beta_2 w}{\beta_2(\alpha_1 + u)} + \frac{\gamma_3 v}{\alpha_2 + v} - \delta_2, & \gamma_2 \beta_2 u > p - \beta_1 v - \beta_2 w, \\ & \gamma_3 \beta_2 \leq \varepsilon \beta_1; \\ \frac{\gamma_2 u}{\alpha_1 + u} + \frac{\varepsilon \beta_1 v}{\beta_2(\alpha_2 + v)} - \delta_2, & \gamma_2 \beta_2 u \leq p - \beta_1 v - \beta_2 w, \\ & \gamma_3 \beta_2 > \varepsilon \beta_1; \\ \frac{p - \beta_1 v - \beta_2 w}{\beta_2(\alpha_1 + u)} + \frac{\varepsilon \beta_1 v}{\beta_2(\alpha_2 + v)} - \delta_2, & \gamma_2 \beta_2 u > p - \beta_1 v - \beta_2 w, \\ & \gamma_3 \beta_2 > \varepsilon \beta_1. \end{array} \right.$$

3.1 Well-posedness

Now, we establish the well-posedness of our model. Let

$$\bar{k} = \min\{k, p\} = \begin{cases} k, & p > k, \\ p, & p \leq k, \end{cases}$$

$$\Omega = \{(u, v, w) : 0 < u < \bar{k}, 0 < v < p/\beta_1, 0 < w < p/\beta_2, u + \beta_1 v + \beta_2 w < p\}.$$

Theorem 3.1 Ω is positive invariant for the semiflow generated by System (3.1).

Proof Let $U(t) = (u(t), v(t), w(t))$ be a solution of System (3.1) with initial condition $U(0) = (u(0), v(0), w(0)) \in \Omega$. We prove the theorem by contradiction. Suppose that there exists a time t_1 such that $U(t_1)$ touches or crosses the boundary of Ω for the first time. To consider the following cases, we let $v_1 = \max_{t \in [0, t_1]} v(t) < p/\beta_1$, $w_1 = \max_{t \in [0, t_1]} w(t) < p/\beta_2$.

Case 1. $u(t_1) = 0$. For every $t \in [0, t_1]$, we have

$$\begin{aligned} \frac{du}{dt} &= u \left(1 - \frac{u}{\min\{k, p - \beta_1 v - \beta_2 w\}} \right) - \frac{uv}{1 + u} - \frac{uw}{\alpha_1 + u} \\ &\geq -\frac{uv}{1 + u} - \frac{uw}{\alpha_1 + u} \\ &\geq -\left(v_1 + \frac{w_1}{\alpha_1} \right) u \equiv \xi_1 u, \end{aligned}$$

where ξ_1 is a constant. Thus $u(t_1) \geq u(0)e^{\xi_1 t_1} > 0$. This contradicts $u(t_1) = 0$, therefore, $U(t_1)$ can not touch this boundary.

Case 2. $v(t_1) = 0$. For every $t \in [0, t_1]$, one has

$$\frac{dv}{dt} = \min \left\{ \gamma_1, \frac{p - \beta_1 v - \beta_2 w}{\beta_1 u} \right\} \frac{uv}{1 + u} - \frac{\varepsilon v w}{\alpha_2 + v} - \delta_1 v$$

$$\begin{aligned} &\geq -\frac{\varepsilon v w}{\alpha_2 + v} - \delta_1 v \\ &\geq -\left(\frac{\varepsilon w_1}{\alpha_2} + \delta_1\right) v \equiv \xi_2 v, \end{aligned}$$

where ξ_2 is a constant. This implies $v(t_1) \geq v(0)e^{\xi_2 t_1} > 0$, which contradicts $v(t_1) = 0$. Thus $U(t_1)$ can not reach this boundary.

Case 3. $w(t_1) = 0$. For every $t \in [0, t_1]$, one has

$$\begin{aligned} \frac{dw}{dt} &= \min\left\{\gamma_2, \frac{p - \beta_1 v - \beta_2 w}{\beta_2 u}\right\} \frac{uw}{\alpha_1 + u} + \min\left\{\gamma_3, \frac{\varepsilon \beta_1}{\beta_2}\right\} \frac{vw}{\alpha_2 + v} - \delta_2 w \\ &\geq -\delta_2 w. \end{aligned}$$

Thus $w(t_1) \geq w(0)e^{-\delta_2 t_1} > 0$. It contradicts $v(t_1) = 0$ and excludes the possibility that $U(t_1)$ touches this boundary.

Case 4. $u(t_1) + \beta_1 v(t_1) + \beta_2 w(t_1) = p$. Note that

$$\begin{aligned} &u \left(1 - \frac{u(t_1)}{\min\{k, p - \beta_1 v(t_1) - \beta_2 w(t_1)\}}\right) \\ &\leq u \left(1 - \frac{u(t_1)}{p - \beta_1 v(t_1) - \beta_2 w(t_1)}\right) = 0, \end{aligned}$$

we have

$$\begin{aligned} &\left. \frac{d(u(t) + \beta_1 v(t) + \beta_2 w(t))}{dt} \right|_{t=t_1} \\ &= \frac{du(t_1)}{dt} + \frac{\beta_1 dv(t_1)}{dt} + \frac{\beta_2 dw(t_1)}{dt} \\ &\leq \min\{\beta_1 \gamma_1 - 1, 0\} \frac{u(t_1)v(t_1)}{1 + u(t_1)} + \min\{\beta_2 \gamma_2 - 1, 0\} \frac{u(t_1)w(t_1)}{\alpha_1 + u(t_1)} \\ &\quad + \min\{\beta_2 \gamma_3 - \varepsilon \beta_1, 0\} \frac{v(t_1)w(t_1)}{\alpha_2 + v(t_1)} - \beta_1 \delta_1 v(t_1) - \beta_2 \delta_2 w(t_1) \\ &\leq 0. \end{aligned}$$

Therefore, $U(t_1)$ can not cross this boundary.

Case 5. $u(t_1) = \bar{k}$. For every $t \in [0, t_1]$, one has

$$\begin{aligned} \frac{du}{dt} &= u \left(1 - \frac{u}{\min\{k, p - \beta_1 v - \beta_2 w\}}\right) - \frac{uv}{1 + u} - \frac{uw}{\alpha_1 + u} \\ &\leq u \left(1 - \frac{u}{\min\{k, p - \beta_1 v - \beta_2 w\}}\right) \\ &\leq u \left(1 - \frac{u}{\min\{k, p\}}\right) \\ &= u \left(1 - \frac{u}{\bar{k}}\right). \end{aligned}$$

Following from the standard comparison argument, we know that $u(t_1) \leq \bar{k}$. Hence $U(t_1)$ can not cross this boundary as well.

All possibilities that $U(t_1)$ touches or crosses the boundary of Ω are excluded. Therefore, set Ω is positive invariant with respect to System (3.1). We thus claim that each solution of System (3.1) with initial condition $U(0) \in \Omega$ stays in Ω for any $t \geq 0$. \square

Note also that Ω is bounded by definition. It follows from this and Theorem 3.1 that solutions of System (3.1) with initial conditions in Ω are bounded.

3.2 Equilibria

3.2.1 Dynamics of boundary equilibria

Obviously, $E_0 = (0, 0, 0)$ and $E_1 = (\bar{k}, 0, 0)$ are two trivial equilibria. Other boundary equilibria are given in the form of $E_2 = (\bar{u}, \bar{v}, 0)$ (the omnivore-absent equilibrium) and $E_3 = (\bar{u}, 0, \bar{w})$ (the herbivore-absent equilibrium).

When the species w is absent, that is $w = 0$, System (3.1) reduces to the following stoichiometric predator–prey system:

$$\begin{cases} \frac{du}{dt} = u \left(1 - \frac{u}{\min\{k, p - \beta_1 v\}} \right) - \frac{uv}{1+u}, \\ \frac{dv}{dt} = \min \left\{ \gamma_1, \frac{p - \beta_1 v}{\beta_1 u} \right\} \frac{uv}{1+u} - \delta_1 v. \end{cases} \quad (3.2)$$

Xie et al. (2018) studied the dynamics of System (3.2) thoroughly. A boundary equilibrium in the form of E_2 corresponds to an interior equilibrium of System (3.2). Following from the results in Xie et al. (2018), we know System (3.2) can have at most 3 interior equilibria. Two types of bistability occur (node–node bistability and node–cycle bistability). Hence, we obtain the result that System (3.1) can have at most 3 boundary equilibria in the form of E_2 .

When the species v is absent, that is $v = 0$, System (3.1) reduces to the following stoichiometric predator–prey system:

$$\begin{cases} \frac{du}{dt} = u \left(1 - \frac{u}{\min\{k, p - \beta_2 w\}} \right) - \frac{uw}{\alpha_1 + u}, \\ \frac{dw}{dt} = \min \left\{ \gamma_2, \frac{p - \beta_2 w}{\beta_2 u} \right\} \frac{uw}{\alpha_1 + u} - \delta_2 w. \end{cases} \quad (3.3)$$

Similarly, System (3.3) can have at most 3 interior equilibria and two types of bistability. Hence, we obtain the result that System (3.1) can have at most 3 boundary equilibria in the form of E_3 .

For the trivial equilibria E_0 and E_1 , we have the following stability result, whose proof is presented in “Appendix 1”.

Theorem 3.2 For System (3.1), equilibrium E_0 is an unstable saddle point, and equilibrium E_1 is unstable if

$$\max \left\{ \frac{\min \left\{ \gamma_1, \frac{p}{\beta_1 k} \right\} \bar{k}}{\delta_1(1 + \bar{k})}, \frac{\min \left\{ \gamma_2, \frac{p}{\beta_2 k} \right\} \bar{k}}{\delta_2(\alpha_1 + \bar{k})} \right\} > 1$$

and is locally asymptotically stable if

$$\max \left\{ \frac{\min \left\{ \gamma_1, \frac{p}{\beta_1 k} \right\} \bar{k}}{\delta_1(1 + \bar{k})}, \frac{\min \left\{ \gamma_2, \frac{p}{\beta_2 k} \right\} \bar{k}}{\delta_2(\alpha_1 + \bar{k})} \right\} < 1.$$

Now, we give a sufficient condition for E_1 to be globally asymptotically stable. Its proof is given in ‘‘Appendix 1’’.

Remark 3.3 Note that if $\max \left\{ \frac{\gamma_1 \bar{k}}{\delta_1(1 + \bar{k})}, \frac{\gamma_2 \bar{k}}{\delta_2(\alpha_1 + \bar{k})} \right\} < 1$, then E_1 is locally asymptotically stable. Moreover, if $\max \left\{ \frac{\gamma_1 \bar{k}}{\delta_1(1 + \bar{k})}, \frac{\gamma_2 \bar{k}}{\delta_2(\alpha_1 + \bar{k})} \right\} < 1$, E_1 is globally asymptotically stable.

Based on the dynamics of the interior equilibria of System (3.2), which were analyzed in Xie et al. (2018), we can also give the following result on the existence of boundary equilibria of System (3.1). This result follows from Theorems 3.1 to 3.7 of Xie et al. in Xie et al. (2018).

Theorem 3.4 System (3.1) can have at most 3 boundary equilibria in the form of E_2 (the omnivore-absent equilibrium), and at most 3 boundary equilibria in the form of E_3 (the herbivore-absent equilibrium). Moreover, System (3.1) may exhibit two types of bistability (node-node bistability and node-cycle bistability).

3.3 Dynamics of interior equilibria

To study the interior equilibria of the stoichiometric model (3.1), we discuss the dynamics when the growth of the plant is limited by light availability and the other two species’ growth rates are limited by carbon. Starting from Model (2.1) and making these assumptions gives us the following model:

$$\begin{cases} \frac{dx}{dt} = rx \left(1 - \frac{x}{K} \right) - \frac{c_1 xy}{a_1 + x} - \frac{c_2 xz}{a_2 + x}, \\ \frac{dy}{dt} = \frac{e_1 c_1 xy}{a_1 + x} - \frac{c_3 yz}{a_3 + y} - d_1 y, \\ \frac{dz}{dt} = \frac{e_2 c_2 xz}{a_2 + x} + \frac{e_3 c_3 yz}{a_3 + y} - d_2 z. \end{cases} \tag{3.4}$$

Let

$$\Omega^* = \{(u, v, w) \in \Omega : k < p - \beta_1 v - \beta_2 w, \gamma_1 \beta_1 u + \beta_1 v + \beta_2 w < p, \gamma_2 \beta_2 u + \beta_1 v + \beta_2 w < p, \gamma_3 \beta_2 < \varepsilon \beta_1\}$$

be the special region in which the growth rates of the plant and the other two species are limited by light availability and carbon, respectively. Also, suppose that we nondimensionalize Model (3.4) in the same way as we did to obtain Model (3.1) earlier, *mutatis mutandis*. Now, we study the existence of interior equilibria of the resulting model, which is as follows:

$$\begin{cases} \frac{du}{dt} = u \left(1 - \frac{u}{k} \right) - \frac{uv}{1+u} - \frac{uw}{\alpha_1+u}, \\ \frac{dv}{dt} = \frac{\gamma_1 uv}{1+u} - \frac{\varepsilon vw}{\alpha_2+v} - \delta_1 v, \\ \frac{dw}{dt} = \frac{\gamma_2 uw}{\alpha_1+u} + \frac{\gamma_3 vw}{\alpha_2+v} - \delta_2 w, \end{cases} \tag{3.5}$$

where the solution $U(t) = (u(t), v(t), w(t)) \in \Omega^*$.

Let

$$S_u = \begin{cases} \left(\frac{\alpha_1(\delta_2 - \gamma_3)}{\gamma_2 + \gamma_3 - \delta_2}, \infty \right), & \max\{\gamma_2, \gamma_3\} < \delta_2 < \gamma_2 + \gamma_3, \\ (0, \infty), & \gamma_2 \leq \delta_2 \leq \gamma_3, \\ \left(\frac{\alpha_1(\delta_2 - \gamma_3)}{\gamma_2 + \gamma_3 - \delta_2}, \frac{\alpha_1 \delta_2}{\gamma_2 - \delta_2} \right), & \gamma_3 < \delta_2 < \gamma_2, \\ \left(0, \frac{\alpha_1 \delta_2}{\gamma_2 - \delta_2} \right), & \delta_2 < \min\{\gamma_2, \gamma_3\}. \end{cases}$$

For System (3.5), we have the following result and present its proof in ‘‘Appendix 1’’.

Theorem 3.5 *Assume $\gamma_1 > \delta_1$, $\gamma_2 + \gamma_3 > \delta_2$, and $S_E = S_u \cap \left(\frac{\delta_1}{\gamma_1 - \delta_1}, k \right) \neq \emptyset$. System (3.5) has at most two interior equilibria $E^* = (u^*, v^*, w^*)$ provided that $E^* \in \Omega^*$. Moreover, System (3.5) admits a saddle-node bifurcation.*

Remark 3.6 Note that System (3.5) is a special case of the stoichiometric system (3.1), in which the limiting factors for the growth of each species are as specified above. From Theorem 3.5, we obtain that the stoichiometric system (3.1) admits at most two interior equilibria within this region. Our proof of this result in ‘‘Appendix 1’’ also holds if System (3.1) is reduced by assuming that $\min\left\{ \gamma_3, \frac{\varepsilon \beta_1}{\beta_2} \right\} = \frac{\varepsilon \beta_1}{\beta_2}$ rather than γ_3 and making all of the other assumptions that were used to produce System (3.5). This is because ε , β_1 , and β_2 are all constants, and γ_3 does not appear in System (3.1) other than in this minimum function, so substituting γ_3 for $\frac{\varepsilon \beta_1}{\beta_2}$ does not change any of the mathematical analysis in the proof. (As the other ways to reduce System (3.1) by choosing specific arguments for its minimum functions leave us with rational functions of all three variables, providing specific conditions for the existence of interior equilibria in other regions is difficult.) In ‘‘Appendix 1’’, we use the Routh–Hurwitz criterion to present a rough sufficient stability condition for a given interior equilibrium of System (3.1), as establishing explicit sufficient stability conditions is difficult due to the system’s complexity. Following this, we choose a set of parameter values to verify this stability condition numerically.

4 Numerical simulations

In aquatic environments, algae (such as phytoplankton) serve as the main primary producers. Through photosynthesis, they provide energy to support organisms elsewhere in an aquatic food web. This includes herbivorous zooplankton such as daphnia (Scheffer et al. 1997), as well as herbivorous and omnivorous fish species (Attayde et al. 2010). Fish taxa like buffalofish and minnows are omnivorous, and hence they can both compete with herbivores for algae and consume the herbivores directly. In this section, we run simulations to illustrate the interactions among three species (a producer, a herbivore and a predator). The parameter values that we used in our simulations are given in Table 2.

Theorem 3.4 shows that the stoichiometric system (2.1) may exhibit two types of bistability at the boundary. This is demonstrated in Figs. 2 and 3. As shown in Fig. 2, node-node bistability occurs, in which two stable boundary equilibria coexist in the xy -plane. In Fig. 3, node-cycle bistability, in which a stable limit cycle coexists with a stable boundary equilibrium in the xy -plane, is visible. Besides these two types of bistability, we also observed others. For instance, instances of both node-node and node-cycle bistability that feature an interior equilibrium are also possible. In Fig. 4, the boundary equilibrium E_2^1 and the interior equilibrium E_2^* are both locally asymptotically stable. Additionally, we see in Fig. 5 both a stable limit cycle lying on the xy -plane and a stable interior equilibrium at E_2^* . Figure 6 demonstrates the occurrence of cycle-cycle bistability: a stable positive limit cycle coexists with a stable

Table 2 Parameters in the stoichiometric System (2.1)

Parameter	Value	References
r	1.2/day	Peace (2015)
K	0–10 mgC/L	Chen et al. (2017, 2018), Heggerud et al. (2020)
P	0.01–0.15 mgP/L	
θ_1	0.03 mgP/mgC	Chen et al. (2017), Peace (2015)
θ_2	0.04 mgP/mgC	Chen et al. (2017, 2018)
q	0.0038 mgP/mgC	Chen et al. (2017), Peace (2015)
a_1	0.25 mgC/L	Chen et al. (2017), Peace (2015)
a_2	0.25 mgC/L	
a_3	0.25 mgC/L	Chen et al. (2017)
c_1	0.81/day	Chen et al. (2017), Peace (2015)
c_2	0.3/day	
c_3	0.81/day	Chen et al. (2017, 2018)
e_1	0.8 (unitless)	Chen et al. (2017), Peace (2015)
e_2	0.8 (unitless)	
e_3	0.8 (unitless)	Chen et al. (2017, 2018)
d_1	0.25/day	Chen et al. (2017, 2018), Peace (2015)
d_2	0.25/day	Chen et al. (2017, 2018)

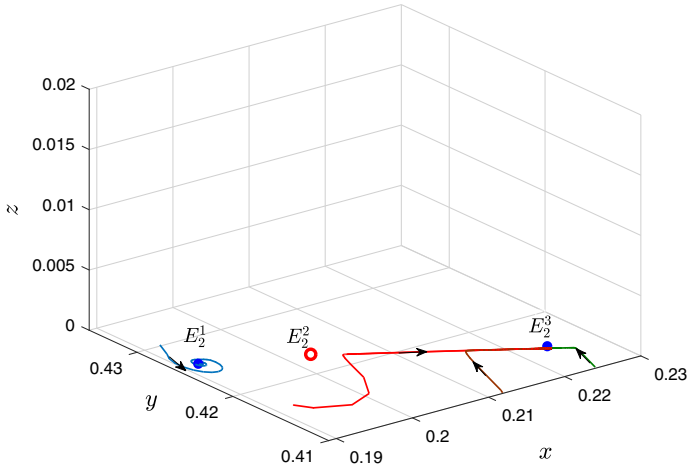


Fig. 2 Node-node bistability. The boundary equilibria E_2^1 and E_2^3 are both stable, while E_2^2 is unstable. Parameter values are: $r = 1.2$; $a_1 = 0.25$; $a_2 = 0.75$; $a_3 = 0.25$; $c_1 = 0.8$; $c_2 = 0.1$; $c_3 = 0.81$; $e_1 = 0.9$; $e_2 = 0.8$; $e_3 = 0.8$; $\theta_1 = 0.04$; $\theta_2 = 0.05$; $d_1 = 0.313$; $d_2 = 0.75$; $q = 0.004$; $P = 0.024$; $K = 0.5372180656$

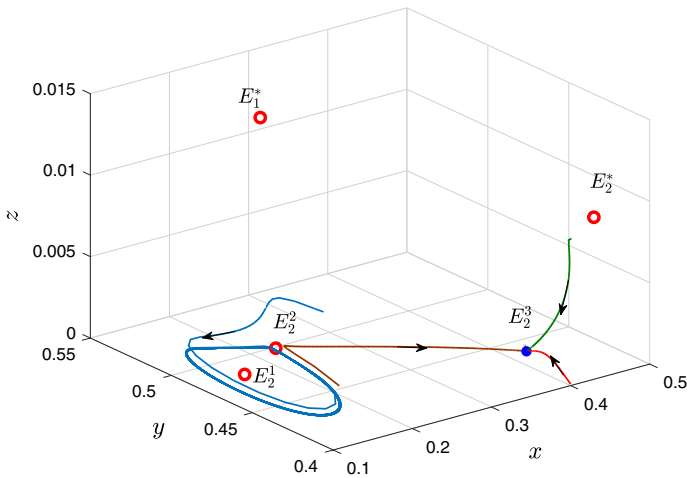


Fig. 3 Node-cycle bistability. A stable limit cycle coexists with a stable boundary equilibrium. The boundary equilibria E_2^1 and E_2^2 are both unstable, while the boundary equilibrium E_2^3 is stable. A stable limit cycle appears around the boundary equilibrium E_2^2 . Parameter values are: $r = 1.2$; $a_1 = 0.25$; $a_2 = 0.75$; $a_3 = 0.25$; $c_1 = 0.8$; $c_2 = 0.3$; $c_3 = 0.8$; $e_1 = 0.8$; $e_2 = 0.8$; $e_3 = 0.85$; $\theta_1 = 0.04$; $\theta_2 = 0.03$; $d_1 = 0.25$; $d_2 = 0.6$; $q = 0.004$; $P = 0.026$; $k = 0.75$

limit cycle in the xy -plane. This type of bistability has been observed in delayed IGP models, but only rarely in IGP models without any delay such as ours.

To illustrate our theoretical results in Theorem 3.5, we plot a bifurcation diagram with K as our chosen bifurcation parameter. As shown in Fig. 7, System (3.4) has no interior equilibria when $K < K^{SN}$. As K increases, a saddle-node bifurcation

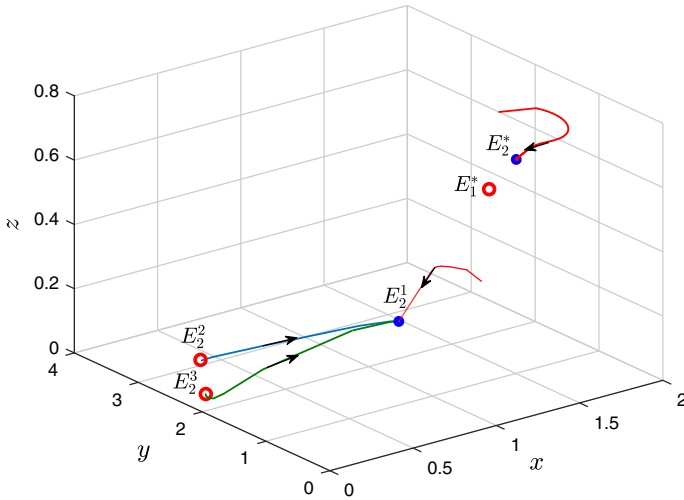


Fig. 4 Node-node bistability. A stable boundary equilibrium coexists with a stable interior equilibrium. The boundary equilibrium E_2^1 and interior equilibrium E_2^* are stable, while other equilibria are unstable. Parameter values are: $r = 5$; $a_1 = 0.25$; $a_2 = 0.55$; $a_3 = 0.25$; $c_1 = 0.8$; $c_2 = 0.4$; $c_3 = 0.5$; $e_1 = 0.8$; $e_2 = 0.4$; $e_3 = 0.3$; $\theta_1 = 0.03$; $\theta_2 = 0.04$; $d_1 = 0.25$; $d_2 = 0.25$; $q = 0.0038$; $P = 0.1$; $K = 2$

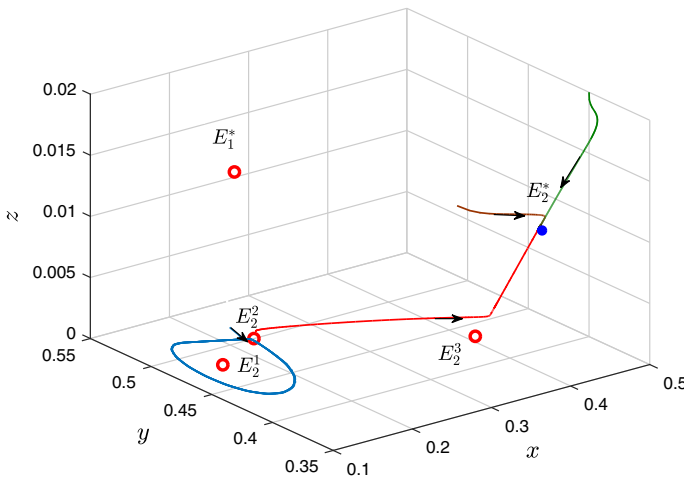


Fig. 5 Node-cycle bistability. A stable limit cycle coexists with a stable interior equilibrium. The interior equilibrium E_2^* is stable, while other equilibria are all unstable. A stable limit cycle appears around the boundary equilibrium E_2^1 . Parameter values are: $r = 1.2$; $a_1 = 0.25$; $a_2 = 0.75$; $a_3 = 0.25$; $c_1 = 0.81$; $c_2 = 0.3$; $c_3 = 0.8$; $e_1 = 0.8$; $e_2 = 0.8$; $e_3 = 0.85$; $\theta_1 = 0.04$; $\theta_2 = 0.03$; $d_1 = 0.25$; $d_2 = 0.5$; $q = 0.004$; $P = 0.026$; $K = 0.75$

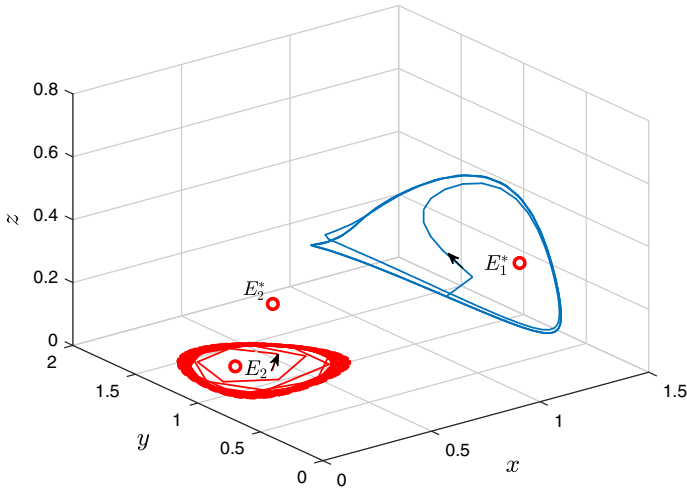


Fig. 6 Cycle-cycle bistability. Two stable limit cycles coexist. Two interior equilibria, as well as a boundary equilibrium E_2 , are all unstable. Two stable limit cycles emerge around the interior equilibrium E_1^* and the boundary equilibrium E_2 . Parameter values are: $r = 5$; $a_1 = 0.4$; $a_2 = 0.5$; $a_3 = 0.6152$; $c_1 = 2.05$; $c_2 = 1.6$; $c_3 = 0.95$; $e_1 = 0.85$; $e_2 = 0.85$; $e_3 = 0.8$; $d_1 = 0.8$; $d_2 = 1.1$; $\theta_1 = 0.03$; $\theta_2 = 0.04$; $q = 0.0038$; $P = 0.25$; $K = 1.2$

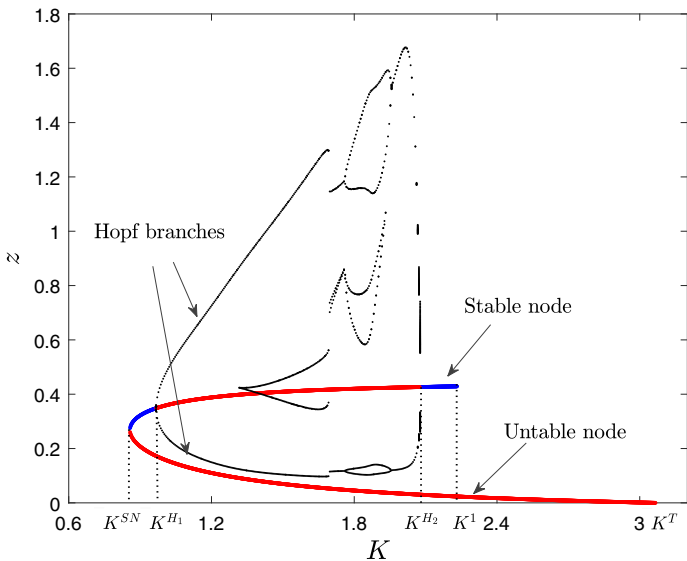


Fig. 7 Bifurcation diagram of System (3.4) with parameters: $r = 5$; $a_1 = 0.4$; $a_2 = 0.5$; $a_3 = 0.6152$; $c_1 = 2.05$; $c_2 = 1.6$; $c_3 = 0.95$; $e_1 = 0.85$; $e_2 = 0.85$; $e_3 = 0.8$; $d_1 = 0.8$; $d_2 = 1.1$. Initial condition: $(x(0), y(0), z(0)) = (0.6, 0.6, 0.32)$

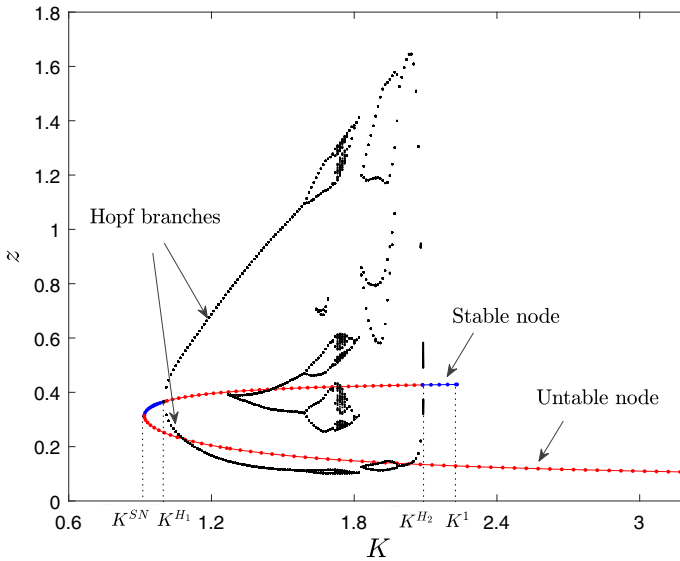


Fig. 8 Bifurcation diagram of the stoichiometric system (2.1) with parameters: $r = 5; a_1 = 0.4; a_2 = 0.5; a_3 = 0.6152; c_1 = 2.05; c_2 = 1.6; c_3 = 0.95; e_1 = 0.85; e_2 = 0.85; e_3 = 0.8; d_1 = 0.8; d_2 = 1.1; \theta_1 = 0.03; \theta_2 = 0.04; q = 0.0038; P = 0.25$. Initial condition: $(x(0), y(0), z(0)) = (0.6, 0.6, 0.32)$

occurs at K^{SN} , and Hopf bifurcations emerge at K^{H1} and K^{H2} . System (3.4) admits two interior equilibria when $K \in (K^{SN}, K^1)$. For $K \in (K^{SN}, K^{H1})$ and (K^{H2}, K^1) , of these two interior equilibria, one is stable and the other is a saddle point. When $K^{H1} < K < K^{H2}$, there are two unstable interior equilibria, while a stable limit cycle emerges around the unstable interior equilibrium. Furthermore, System (3.4) has a unique unstable interior equilibrium for $K \in (K^1, K^T)$. As K further increases to K^T , a transcritical bifurcation occurs and the unstable interior equilibrium disappears. Past this point, System (3.4) admits no interior equilibria.

Due to the complexity of the stoichiometric system (2.1), we will restrict our analysis of the interior equilibrium to numerical results. Figure 8 indicates that the dynamics of the stoichiometric system (2.1) are similar to those of System (3.4) when $K < K^{H1}$. When K is larger than K^{H1} , the stoichiometric system has periodic solutions oscillating around an unstable interior equilibrium, as with the nonstoichiometric one. However, a key difference between them is that chaos appears in the stoichiometric system through a period doubling cascade for increasing K . As K is further increased, the chaos disappears and periodic solutions emerge again. These periodic solutions disappear when K passes K^{H2} , and the interior equilibrium becomes stable. When K passes K^1 , the stoichiometric system (2.1) admits a unique unstable interior equilibrium. It can be seen in Fig. 8 that including stoichiometry in the model leads to complex dynamics, such as the destabilization of the system (3.4).

In the following subsections, we explore how the stoichiometric system (2.1) responds to variations in light intensity K and nutrient availability P , taking K and P as bifurcation parameters.

4.1 Effects of light intensity

Now, we explore the effect of light intensity on dynamical behaviors. We plot bifurcation diagrams of System (3.4) to study the effect of light on system dynamics. As shown in Fig. 9, when K is tiny, light intensity is low enough so that the plant cannot provide enough energy to support the growth of the herbivore and omnivore (which thus cannot survive due to starvation). For this reason, System (3.4) has no interior equilibria, while the boundary equilibrium $(K, 0, 0)$ is stable. With increasing K , more energy input makes the herbivore and omnivore survive, and hence a stable interior equilibrium appears. At this equilibrium, the three species coexist at constant densities. When $K = 0.27$, System (3.4) undergoes a Hopf bifurcation. As K passes 0.27, due to the Hopf bifurcation, the positive equilibrium loses its stability and a stable limit cycle emerges, in which the three species coexist at regular oscillatory densities. Increasing K further causes the paradox of enrichment to be observed. For $K > 0.92$, the herbivore-absent equilibrium becomes stable; when this is the case, the herbivore goes to extinction and the three species cannot coexist. When $K > 2$, the herbivore-absent equilibrium loses its stability and a stable limit cycle emerges around it, which features the plant and omnivore populations oscillating periodically. In summary, as light intensity is increased, plant density increases through its entire range of possible values, but high densities result in the extinction of the herbivore.

The incorporation of stoichiometry, i.e. taking the system to be (2.1), causes more complicated and richer dynamics to take place. Under very low light availability, the plant's growth is limited by light intensity. In contrast, high light availability leads to the plant's growth being limited by the amount of nutrients in the environment.

We first explore the dynamics of the stoichiometric system (2.1) in low nutrient environments ($P = 0.04$). From the bifurcation diagram presented in Fig. 10, we notice that when $K < 0.98$, the dynamics of the stoichiometric system (2.1) is similar to that of System (3.4). As K increases through a threshold value ($K = 0.98$), the dynamics of System (2.1) show great differences compared to those of the nonstoichiometric system. We observe for $K \in (0.98, 1.24)$ that the biomass of the omnivore decreases due to very few herbivores to consume. If K increases further, the plant's growth is limited by nutrient conditions rather than light intensity. When K passes 1.24, the previously severely endangered herbivore starts to survive, leading to an interior equilibrium featuring all three species. With a further increasing of K , the stoichiometric system (2.1) undergoes a Hopf bifurcation again ($K = 1.48$), after which all species coexist in an oscillatory fashion (in the range $1.48 < K < 1.52$). Beyond this lies a brief window for K that features a stable interior equilibrium again, followed by all-species oscillatory coexistence for $1.57 < K < 2.83$. When $2.83 < K < 3.83$, the stoichiometric system (2.1) returns to exhibiting a stable interior equilibrium. For values of K that are higher than this, the omnivore goes extinct due to low nutrient condition, and the biomass of the herbivore first begins to decrease and the goes to zero as well (for sufficiently large K). In summation, under high light and low nutrient conditions, the plant's quality as a food source is low due to the imbalance of nutrients within it. This leads to low herbivore and omnivore growth, and potentially to extinc-

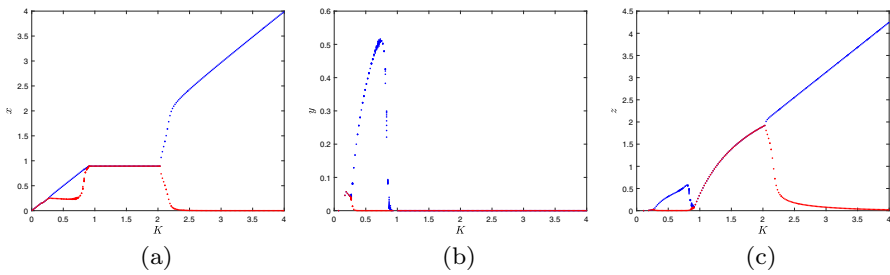


Fig. 9 Bifurcation diagram of System (3.4) with varying K . Other parameter values are $r = 1.2; a_1 = 0.25; a_2 = 0.25; a_3 = 0.25; c_1 = 0.81; c_2 = 0.4; c_3 = 0.81; e_1 = 0.8; e_2 = 0.8; e_3 = 0.8; d_1 = 0.25; d_2 = 0.25$. Initial condition: $(x(0), y(0), z(0)) = (0.2, 0.14, 0.1)$

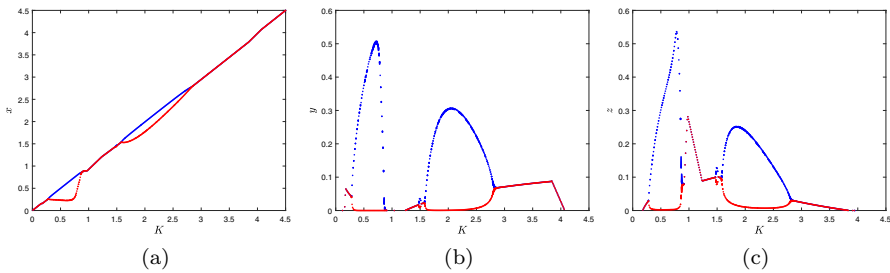


Fig. 10 Bifurcation diagram of the stoichiometric system (2.1) with varying K . Other parameter values are $r = 1.2; a_1 = 0.25; a_2 = 0.25; a_3 = 0.25; c_1 = 0.81; c_2 = 0.4; c_3 = 0.81; e_1 = 0.8; e_2 = 0.8; e_3 = 0.8; \theta_1 = 0.03; \theta_2 = 0.04; d_1 = 0.25; d_2 = 0.25; q = 0.0038; P = 0.04$. Initial condition: $(x(0), y(0), z(0)) = (0.2, 0.14, 0.1)$

tion of both species. Importantly, we find that the omnivore becomes extinct at lower light intensities than the herbivore.

Now, we discuss the dynamics of the stoichiometric system (2.1) in a high nutrient environment. From Fig. 11, we observe that for low intensity of light K , the growth of the plant is limited by light, and hence the dynamical behavior of the stoichiometric system (2.1) is similar to that of System (3.4) for K small. When K passes 3.23, the previously severely endangered herbivore emerges again with healthier population levels. Hence, as the light intensity increases past this value, there exists a stable interior equilibrium. The stoichiometric system (2.1) admits a Hopf bifurcation at $K = 3.43$, at which point a stable limit cycle emerges and the three species coexist in an oscillatory pattern. In high light conditions, the plant’s growth becomes limited by nutrient availability; this allows for greater biomass of all three species, as the herbivore and omnivore have access to good-quality food. For extremely high light intensity ($K > 3.88$), chaos appears, and all populations oscillate irregularly. However, increasing K even further shifts the system into first stable limit cycles, then a stable equilibrium. We can therefore see both destabilization and (eventually) stabilization of the system with increasing light intensity.

For the nonstoichiometric IGP system, we observe chaos, i.e. coexistence of species at irregular oscillatory densities. Figure 12 suggests that our system (3.4) has chaotic dynamics. When K is very small, the boundary equilibrium $(K, 0, 0)$ is stable, as the

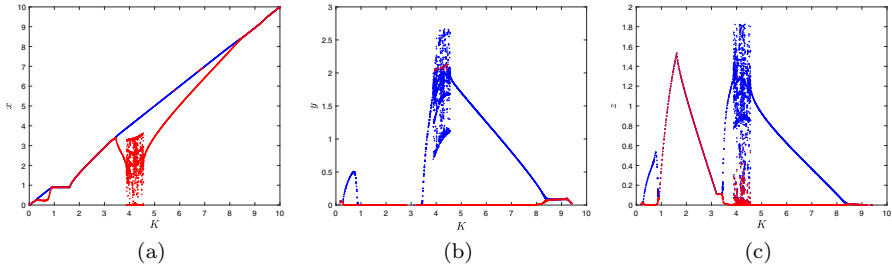


Fig. 11 Bifurcation diagram of the stoichiometric system (2.1) with varying K . Other parameter values are $r = 1.2$; $a_1 = 0.25$; $a_2 = 0.25$; $a_3 = 0.25$; $c_1 = 0.81$; $c_2 = 0.4$; $c_3 = 0.81$; $e_1 = 0.8$; $e_2 = 0.8$; $e_3 = 0.8$; $\theta_1 = 0.03$; $\theta_2 = 0.04$; $d_1 = 0.25$; $d_2 = 0.25$; $q = 0.0038$; $P = 0.09$. Initial condition: $(x(0), y(0), z(0)) = (0.2, 0.14, 0.1)$

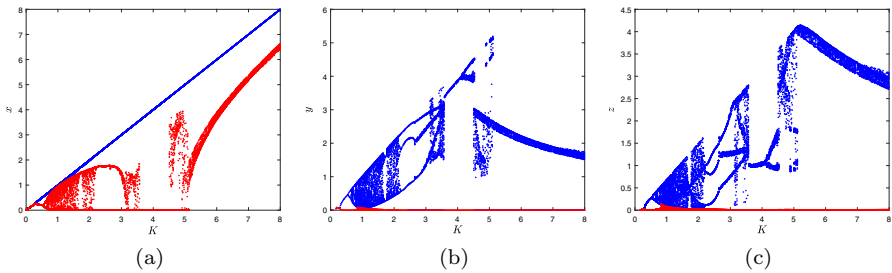


Fig. 12 Bifurcation diagram of System (3.4) with varying K . Other parameter values $r = 1.2$; $a_1 = 0.25$; $a_2 = 0.25$; $a_3 = 0.25$; $c_1 = 0.81$; $c_2 = 0.3$; $c_3 = 0.81$; $e_1 = 0.8$; $e_2 = 0.8$; $e_3 = 0.8$; $d_1 = 0.25$; $d_2 = 0.25$. Initial condition: $(x(0), y(0), z(0)) = (0.2, 0.14, 0.1)$

light intensity is not enough to create a plant density that will sustain the herbivore and omnivore. As the light intensity K increases, the herbivore and then the omnivore start to survive, so that the system briefly reaches an interior stable state, followed by a Hopf bifurcation at $K = 0.29$ that results in periodic solutions where all species coexist. Further increasing K causes chaotic solutions to appear for a large range of values for light intensity ($0.66 < K < 2.23$), after which the chaotic solutions disappear and periodic solutions return. From this bifurcation diagram, we observe that solutions to the system are nearly always oscillatory, and the oscillations are often irregular.

Now, we explore how introducing stoichiometry affects the dynamics of our system under different nutrient environments. In Fig. 13, we analyze the dynamical behavior of the stoichiometric system (2.1) with respect to light intensity K under a low nutrient environment ($P = 0.02$). As we can see, the dynamics of the stoichiometric system (2.1) are similar to that of System (3.4) for low light intensity, although this similarity ends when K passes the threshold value 0.66. Unlike the chaos shown in Fig. 12, increasing light intensity K here instead causes a stable interior equilibrium to appear, so that the three species coexist at constant levels when $0.66 < K < 1.62$. This means that in this case, stoichiometry stabilizes the model dynamics. For $K > 1.62$, the biomass of herbivore starts to decrease, and extinction happens for first the omnivore and then the herbivore; the latter event happens at $K = 1.9$. Here, high light intensity

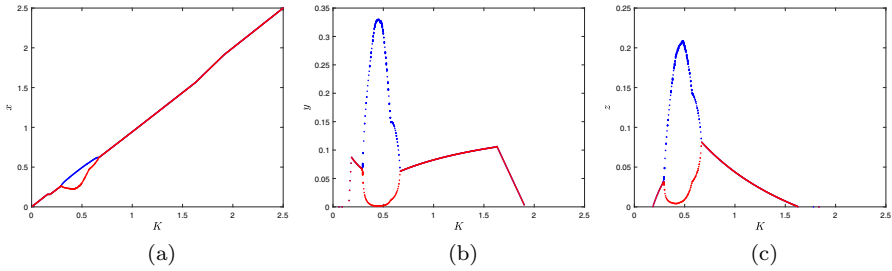


Fig. 13 Bifurcation diagram of the stoichiometric system (2.1) with parameters: $r = 1.2$; $a_1 = 0.25$; $a_2 = 0.25$; $a_3 = 0.25$; $c_1 = 0.81$; $c_2 = 0.3$; $c_3 = 0.81$; $e_1 = 0.8$; $e_2 = 0.8$; $e_3 = 0.8$; $\theta_1 = 0.03$; $\theta_2 = 0.04$; $d_1 = 0.25$; $d_2 = 0.25$; $q = 0.0038$; $P = 0.02$. Initial condition: $(x(0), y(0), z(0)) = (0.2, 0.14, 0.1)$

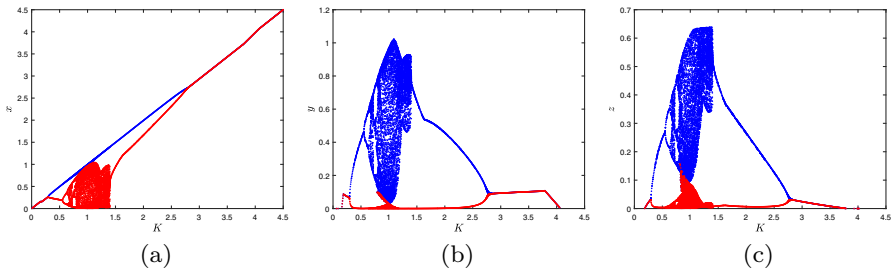


Fig. 14 Bifurcation diagram of the stoichiometric system (2.1) with parameters: $r = 1.2$; $a_1 = 0.25$; $a_2 = 0.25$; $a_3 = 0.25$; $c_1 = 0.81$; $c_2 = 0.3$; $c_3 = 0.81$; $e_1 = 0.8$; $e_2 = 0.8$; $e_3 = 0.8$; $\theta_1 = 0.03$; $\theta_2 = 0.04$; $d_1 = 0.25$; $d_2 = 0.25$; $q = 0.0038$; $P = 0.04$. Initial condition: $(x(0), y(0), z(0)) = (0.2, 0.14, 0.1)$

and low nutrient levels cause an imbalance in the available nutrients for the herbivore and omnivore, which directly leads to their extinction.

To verify that different levels of nutrient availability may lead to different solution behaviours, we take $P = 0.04$ and plot the bifurcation diagram of the stoichiometric system (2.1) with regards to K in Fig. 14. As can be seen from Fig. 14, taking slightly different values of P greatly affects the system dynamics. The diagram shows that the stoichiometric system (2.1) exhibits similar dynamics for low light intensity ($K < 0.67$) as seen previously. However, when $K \in (0.67, 1.41)$, chaos appears, unlike in the case where $P = 0.02$. When K is in the range $(1.41 < K < 2.78)$, the chaos disappears and all solutions tend to a stable limit cycle. After this, as K is increased to values in the range $2.78 < K < 3.78$, the positive equilibrium regains its stability. The three species can coexist in these three cases. Increasing K beyond this makes the system dynamics revert to the pattern seen previously: the interior equilibrium disappears and the boundary equilibrium becomes stable, resulting in the extinction of the herbivore and omnivore.

We also calculate the Lyapunov exponents of the system to demonstrate that chaos occurs. As presented in Fig. 15, we observe the maximal Lyapunov exponent is positive when $K \in (0.67, 1.41)$. In order to better describe the changes in the solution behaviour with respect to light intensity, we plot the solution trajectories in the yz -plane for several different values of K in Fig. 16. Figure 16a–d reveals that chaos appears through a period doubling cascade.

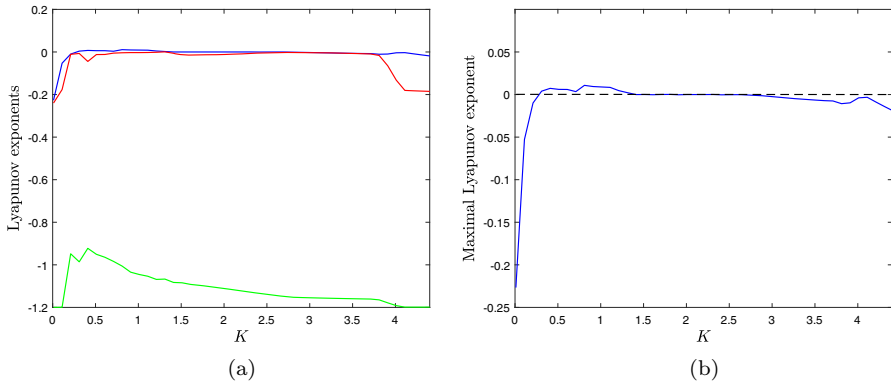


Fig. 15 Spectrum of the Lyapunov exponent as a function of K with parameters: $r = 1.2$; $a_1 = 0.25$; $a_2 = 0.25$; $a_3 = 0.25$; $c_1 = 0.81$; $c_2 = 0.3$; $c_3 = 0.81$; $e_1 = 0.8$; $e_2 = 0.8$; $e_3 = 0.8$; $\theta_1 = 0.03$; $\theta_2 = 0.04$; $d_1 = 0.25$; $d_2 = 0.25$; $q = 0.0038$; $P = 0.04$. Initial condition: $(x(0), y(0), z(0)) = (0.2, 0.14, 0.1)$

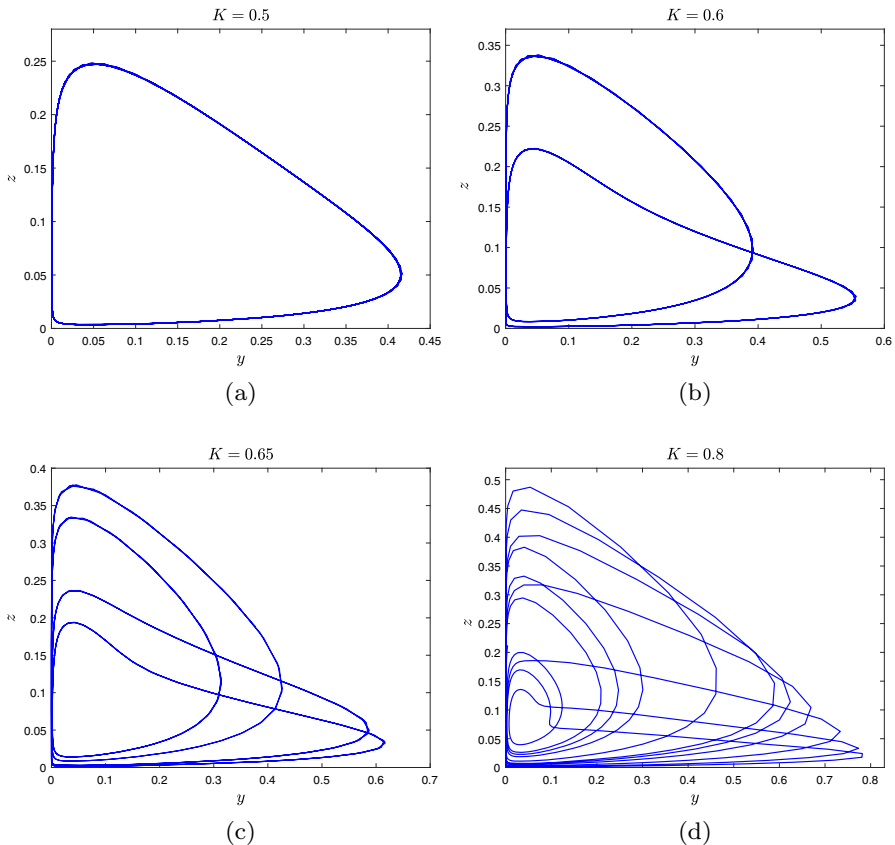


Fig. 16 Chaotic and period-doubling solutions. Parameter values are: $r = 1.2$; $a_1 = 0.25$; $a_2 = 0.25$; $a_3 = 0.25$; $c_1 = 0.81$; $c_2 = 0.3$; $c_3 = 0.81$; $e_1 = 0.8$; $e_2 = 0.8$; $e_3 = 0.8$; $\theta_1 = 0.03$; $\theta_2 = 0.04$; $d_1 = 0.25$; $d_2 = 0.25$; $q = 0.0038$; $P = 0.04$. Initial condition: $(x(0), y(0), z(0)) = (0.2, 0.14, 0.1)$

4.2 Effects of nutrient levels

In this subsection, we study the effects of varying nutrient levels on the dynamics of the stoichiometric system (2.1). We first consider the case with low light intensity ($K = 1.5$): a bifurcation diagram of P under these conditions is shown in Fig. 17. There, we can see that the boundary equilibrium $(K, 0, 0)$ is stable for small values of P . In this case, extremely low nutrient availability leads to low quality food, which cannot support the survival of the herbivore and omnivore. With the increasing of the level of the nutrient input P , the herbivore starts to survive ($P > 0.016$), followed by the omnivore ($P > 0.019$). If $P \in (0.019, 0.029)$, the stoichiometric system (2.1) has a stable interior equilibrium in which three species coexist. Due to the occurrence of a Hopf bifurcation at $P = 0.029$, the positive interior equilibrium loses its stability there, and a stable limit cycle is created. If $P > 0.042$, chaos emerges and persists. This figure suggests that as P increases, the plant can serve as higher-quality food. Hence, increasing P causes the herbivore and omnivore to survive and coexist in three distinct patterns, namely (i) constant densities, (ii) regular oscillatory densities, and (iii) irregular oscillatory densities.

Following this, we explore how variation in nutrient level induces richer model dynamics under medium light intensity ($K = 4$), with our results here shown in Fig. 18. As previously, for small values of P , low food quality means that the herbivore

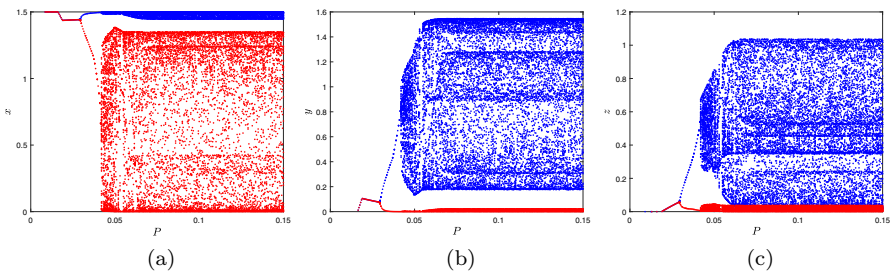


Fig. 17 Bifurcation diagram of the stoichiometric system (2.1) with parameters: $r = 1.2; a_1 = 0.25; a_2 = 0.25; a_3 = 0.25; c_1 = 0.81; c_2 = 0.3; c_3 = 0.81; e_1 = 0.8; e_2 = 0.8; e_3 = 0.8; \theta_1 = 0.03; \theta_2 = 0.04; d_1 = 0.25; d_2 = 0.25; q = 0.0038; K = 1.5$. Initial condition: $(x(0), y(0), z(0)) = (0.2, 0.14, 0.1)$

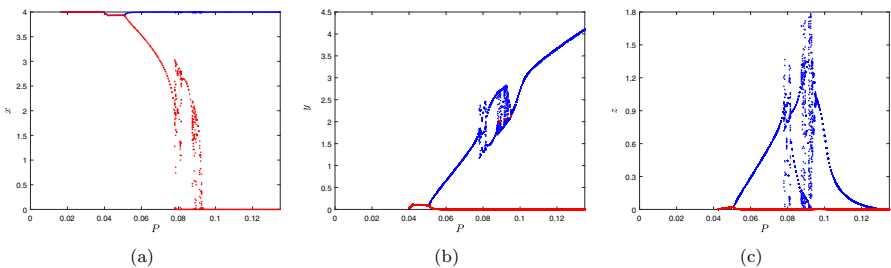


Fig. 18 Bifurcation diagram of the stoichiometric system (2.1) with parameters: $r = 1.2; a_1 = 0.25; a_2 = 0.25; a_3 = 0.25; c_1 = 0.81; c_2 = 0.3; c_3 = 0.81; e_1 = 0.8; e_2 = 0.8; e_3 = 0.8; \theta_1 = 0.03; \theta_2 = 0.04; d_1 = 0.25; d_2 = 0.25; q = 0.0038; K = 4$. Initial condition: $(x(0), y(0), z(0)) = (0.2, 0.14, 0.1)$

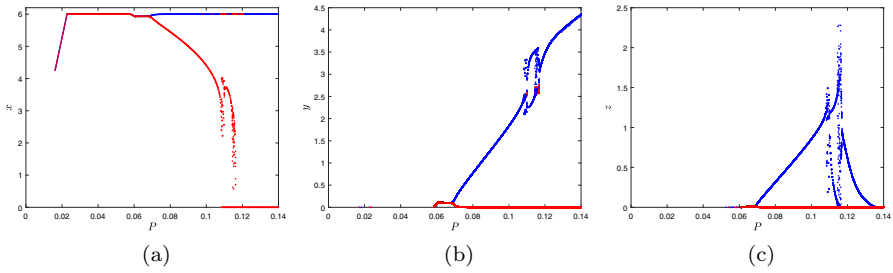


Fig. 19 Bifurcation diagram of the stoichiometric system (2.1) with parameters: $r = 1.2$; $a_1 = 0.25$; $a_2 = 0.25$; $a_3 = 0.25$; $c_1 = 0.81$; $c_2 = 0.3$; $c_3 = 0.81$; $e_1 = 0.8$; $e_2 = 0.8$; $e_3 = 0.8$; $\theta_1 = 0.03$; $\theta_2 = 0.04$; $d_1 = 0.25$; $d_2 = 0.25$; $q = 0.0038$; $K = 6$. Initial condition: $(x(0), y(0), z(0)) = (0.2, 0.14, 0.1)$

and omnivore populations cannot grow in the long-term. As P increases to 0.042, the growth of the herbivore and omnivore populations is constrained by food quality; eventually, the herbivore and omnivore begin to survive and coexist at constant levels. System (2.1) admits a Hopf bifurcation at $P = 0.051$, at which point a stable limit cycle is born. Further increases in P lead first to the occurrence of chaos, and then to the re-emergence of limit cycles. If P is beyond a threshold value ($P > 0.13$), the omnivore cannot survive, and the populations of the two remaining species oscillate around an unstable omnivore-absent equilibrium. Extremely high nutrient condition (i.e. high plant quality) leads to the extinction of omnivore. This is due to the consumption of the plant being monopolized by the herbivore, to the detriment of the omnivore.

Lastly, we discuss the effects of varying nutrient levels on the dynamics of the system under high light intensity ($K = 6$). The extremely high light conditions cause the plant's growth to be limited by P . Thus, small values of P cause the plant to be a poor-quality food source, which constrains the growth of the herbivore as well as the growth and predation of the omnivore. As illustrated in Fig. 19, when P is very small, the herbivore and omnivore cannot survive. As P increases, so does the biomass and quality of the plant. Further increasing P causes the three species to show similar dynamics under high light intensity as they do under medium light intensity. When P is very high, the plant is a high-quality food source, which supports the survival of both the herbivore and omnivore (thus facilitating species coexistence). However, extremely high nutrient conditions result in the extinction of the omnivore, as in the case with medium light intensity.

5 A changing environment

The IGP system that we have analyzed in previous sections can show significantly altered behaviour when the environment changes over time, with the rate of environmental change being a strong determinant of this behaviour. In this section, we investigate the effect of the environmental change rate (μ). From the fourth equation of System (2.2) for K , we can easily determine that the equation for K has the explicit solution $K(t) = K(0) + \mu t$.

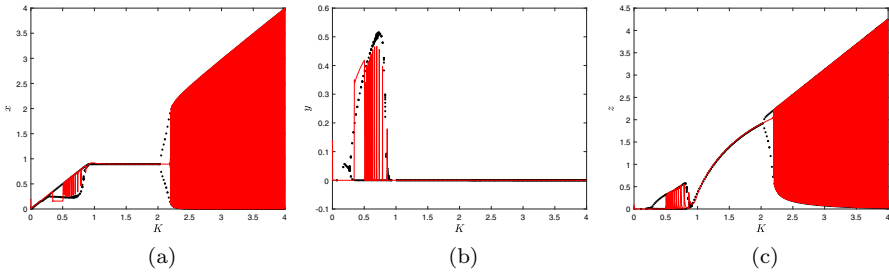


Fig. 20 Rate-dependent dynamics of System (5.1). All equilibria are represented by black curves, while the time series in the temporally varying environment is represented by red curves. Parameter values are: $r = 1.2$; $a_1 = 0.25$; $a_2 = 0.25$; $a_3 = 0.25$; $c_1 = 0.81$; $c_2 = 0.4$; $c_3 = 0.81$; $e_1 = 0.8$; $e_2 = 0.8$; $e_3 = 0.8$; $d_1 = 0.25$; $d_2 = 0.25$; $\mu = 0.0001$. Initial condition: $(x(0), y(0), z(0)) = (0.2, 0.14, 0.1)$ and $K(0) = 0.01$

In our exploration of environmental change, we will first look at the effect of μ on the nonstoichiometric IGP model, which is given as follows:

$$\begin{cases} \frac{dx}{dt} = rx \left(1 - \frac{x}{K}\right) - f(x)y - g(x)z, \\ \frac{dy}{dt} = e_1 f(x)y - h(y)z - d_1 y, \\ \frac{dz}{dt} = e_2 g(x)z + e_3 h(y)z - d_2 z, \\ \frac{dK}{dt} = \mu. \end{cases} \tag{5.1}$$

Now, we study the dynamics of IGP model (5.1) in a time-varying environment, choosing a small change rate $\mu = 0.0001$. As shown in Fig. 20, we observe that the system can track unstable states. Specifically, when K is tiny, System (5.1) admits a transcritical bifurcation; as System (5.1) crosses the transcritical bifurcation point, the boundary equilibrium $(K, 0, 0)$ becomes unstable, but the system tracks the now-unstable boundary equilibrium $(K, 0, 0)$. This behaviour continues as K passes the first Hopf bifurcation point $K = 0.27$ (at which the interior equilibrium becomes unstable), up until $K > 0.5$ when the system instead starts to follow periodic oscillations around the unstable interior equilibrium. Later, as the system crosses the bifurcation point $K = 2$, the herbivore-absent equilibrium becomes unstable and the system takes some time before it switches to exhibiting stable periodic oscillations. During this time, it tracks the unstable herbivore-absent equilibrium, until $K > 2.2$ when stable oscillations emerge.

To explore the effect of the rate of environmental change, we take $\mu = 0.001$ in Fig. 21. The resulting dynamics, as presented in Fig. 21, are similar to those mentioned above. When K passes the transcritical bifurcation point, the system tracks unstable boundary equilibrium $(K, 0, 0)$, and when $K > 2$ (after the Hopf bifurcation), the system tracks the unstable herbivore-absent equilibrium. However, we notice that the tracking appears to last longer for the higher value of μ , and the system follows the stable oscillations for larger K ($K = 2.68$).

We additionally analyze the dynamics of a stoichiometric IGP model (2.1) in a varying environment. We start our analysis of this model by taking $\mu = 0.0001$; the dynamics can be seen in Fig. 22. As with the non-stoichiometric model, System (2.2)

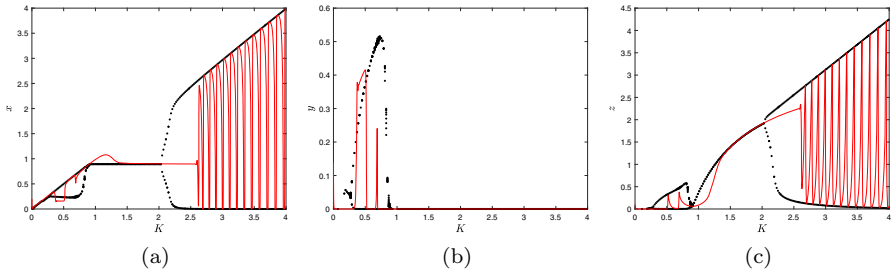


Fig. 21 Rate-dependent dynamics of System (5.1). All equilibria are represented by black curves, while the time series in the temporally varying environment is represented by red curves. Parameter values are: $r = 1.2$; $a_1 = 0.25$; $a_2 = 0.25$; $a_3 = 0.25$; $c_1 = 0.81$; $c_2 = 0.4$; $c_3 = 0.81$; $e_1 = 0.8$; $e_2 = 0.8$; $e_3 = 0.8$; $d_1 = 0.25$; $d_2 = 0.25$; $\mu = 0.001$. Initial condition: $(x(0), y(0), z(0)) = (0.2, 0.14, 0.1)$ and $K(0) = 0.01$ (color figure online)

tracks the unstable boundary equilibrium $(K, 0, 0)$ after the first transcritical bifurcation. When K passes the second transcritical bifurcation, the solution first tracks the unstable herbivore-absent equilibrium ($1.24 < K < 1.4$), then immediately switches to tracking the unstable boundary equilibrium $(K, 0, 0)$ ($1.4 < K < 1.55$) (Fig. 23).

In Fig. 24, we choose a higher environmental change rate ($\mu = 0.001$) for the stoichiometric IGP model. We notice that the solution of System (2.2) tracks the unstable boundary equilibrium $(K, 0, 0)$ when carrying capacity is small. With increasing K , the solution tracks first the unstable herbivore-absent equilibrium (after the second transcritical bifurcation), then the boundary equilibrium $(K, 0, 0)$. We observe that increasing μ causes the system to track the unstable state for longer ($1.26 < K < 1.68$), with a larger value of K ($K = 1.68$) necessary to transition the system to stable oscillations.

Our simulations illustrate that an IGP system with a changing environment can track states which are unstable in the corresponding constant environment. During our numerical simulations, we observed another interesting phenomenon that the tracking of an unstable state depends on the initial condition for the environment. For example, when taking $K(0) = 0.012$ (very close to 0.01), as shown in Fig. 23, the system tracks the unstable boundary equilibria after the second transcritical bifurcation. It therefore does not switch to exhibiting stable oscillations or tracking the coexistence steady state or omnivore-absent equilibrium. In addition, altering the rate of environmental change also results in different tracking results. This is illustrated in Fig. 25, in which we choose two change rates ($\mu = 0.001$ and $\mu = 0.0001$). When $\mu = 0.0001$, the environmental changes are slow, and the system keeps tracking the unstable boundary equilibrium $(K, 0, 0)$ after the transcritical bifurcation. When $\mu = 0.001$, the environment changes more quickly. This results in the system first tracking the unstable boundary equilibrium $(K, 0, 0)$ after the transcritical bifurcation, then switching after the Hopf bifurcation to track the unstable omnivore-absent equilibrium and subsequently follow stable oscillations.

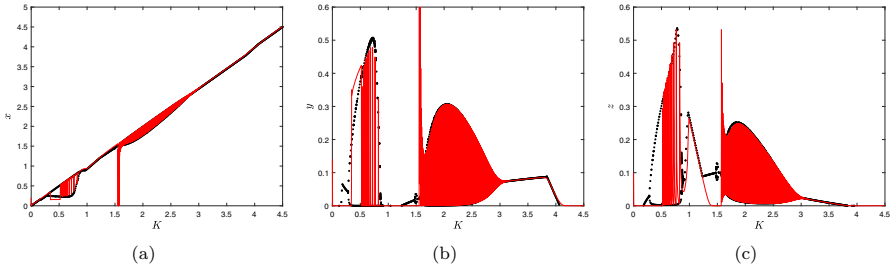


Fig. 22 Rate-dependent dynamics of System (2.2). All equilibria are represented by black curves, while the time series in the temporally varying environment is represented by red curves. Parameter values are: $r = 1.2$; $a_1 = 0.25$; $a_2 = 0.25$; $a_3 = 0.25$; $c_1 = 0.81$; $c_2 = 0.4$; $c_3 = 0.81$; $e_1 = 0.8$; $e_2 = 0.8$; $e_3 = 0.8$; $\theta_1 = 0.03$; $\theta_2 = 0.04$; $d_1 = 0.25$; $d_2 = 0.25$; $q = 0.0038$; $P = 0.04$; $\mu = 0.0001$. Initial condition: $(x(0), y(0), z(0)) = (0.2, 0.14, 0.1)$ and $K(0) = 0.01$ (color figure online)

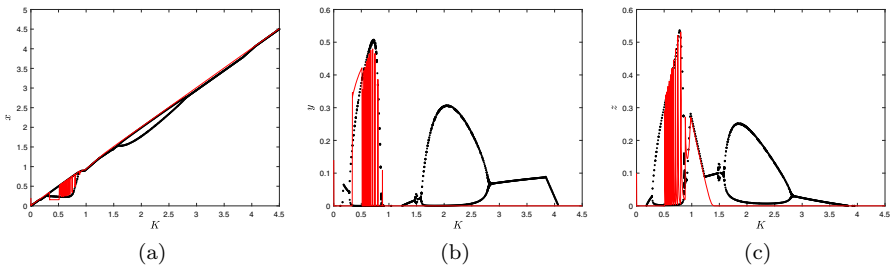


Fig. 23 Rate-dependent dynamics of System (2.2). All equilibria are represented by black curves, while the time series in the temporally varying environment is represented by red curves. Parameter values are: $r = 1.2$; $a_1 = 0.25$; $a_2 = 0.25$; $a_3 = 0.25$; $c_1 = 0.81$; $c_2 = 0.4$; $c_3 = 0.81$; $e_1 = 0.8$; $e_2 = 0.8$; $e_3 = 0.8$; $\theta_1 = 0.03$; $\theta_2 = 0.04$; $d_1 = 0.25$; $d_2 = 0.25$; $q = 0.0038$; $P = 0.04$; $\mu = 0.0001$. Initial condition: $(x(0), y(0), z(0)) = (0.2, 0.14, 0.1)$ and $K(0) = 0.012$ (color figure online)

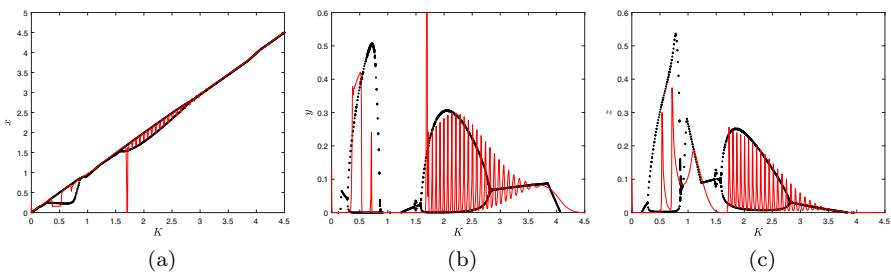


Fig. 24 Rate-dependent dynamics of System (2.2). All equilibria are represented by black curves, while the time series in the temporally varying environment is represented by red curves. Parameter values are: $r = 1.2$; $a_1 = 0.25$; $a_2 = 0.25$; $a_3 = 0.25$; $c_1 = 0.81$; $c_2 = 0.4$; $c_3 = 0.81$; $e_1 = 0.8$; $e_2 = 0.8$; $e_3 = 0.8$; $\theta_1 = 0.03$; $\theta_2 = 0.04$; $d_1 = 0.25$; $d_2 = 0.25$; $q = 0.0038$; $P = 0.04$; $\mu = 0.001$. Initial condition: $(x(0), y(0), z(0)) = (0.2, 0.14, 0.1)$ and $K(0) = 0.01$ (color figure online)

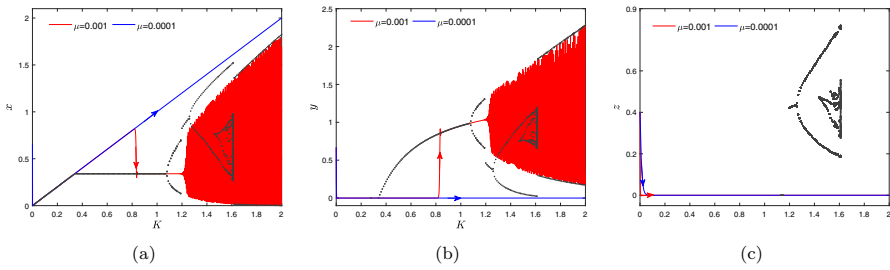


Fig. 25 The numerical solution to System (2.2). All equilibria are represented by black curves, while time series in the temporally varying environment are represented by red and blue curves. Parameter values are: $r = 4$; $a_1 = 0.4$; $a_2 = 0.5$; $a_3 = 0.6152$; $c_1 = 2.05$; $c_2 = 1.5$; $c_3 = 0.95$; $e_1 = 0.85$; $e_2 = 0.85$; $e_3 = 0.8$; $\theta_1 = 0.03$; $\theta_2 = 0.04$; $d_1 = 0.8$; $d_2 = 1.1$; $q = 0.0038$; $P = 0.15$. Initial condition: $(x(0), y(0), z(0)) = (0.66, 0.67, 0.4)$ and $K(0) = 0.001$ (color figure online)

6 Discussion

In this paper, we proposed a novel stoichiometric IGP model. We compared the dynamics of this model with that of a nonstoichiometric version. We derived that the nonstoichiometric IGP model admits at most two interior equilibria, along with saddle-node, Hopf and transcritical bifurcations. We also observed the chaos that often appears in the IGP model. For the nonstoichiometric IGP model, we found that the plant cannot support the survival of the herbivore and omnivore under conditions of very low light intensity. For moderate levels of light intensity, the three species can survive successfully, and they can coexist in three different modes. These are the following: (i) all species populations are maintained at constant levels (corresponding to a stable interior equilibrium); (ii) species populations oscillate periodically (corresponding to a stable limit cycle); and (iii) species populations oscillate irregularly (corresponding to the occurrence of chaos). Extremely high light intensity destabilized the system, resulting in the extinction of the herbivore; this result corresponds to the paradox of enrichment.

We also performed numerical analysis on the stoichiometric IGP model. Within the bifurcation diagrams that we created, we observed multistability; this comprised different kinds of bistability, such as node-node, node-cycle and cycle-cycle bistability. It has been shown that time delay can induce cycle-cycle bistability in IGP models (Shu et al. 2015), but this phenomenon of bistability has not previously been observed in IGP models without delay. This model also exhibited different types of bifurcations (saddle-node and Hopf), as well as chaos. Our numerical results on the effects of light intensity and nutrient availability in the stoichiometric IGP model revealed that both of these have a great impact on the growth and coexistence of the three species. When the total phosphorus availability P is fixed and light intensity is low (specifically low enough that it serves as the limiting factor for plant carrying capacity), the dynamics of the stoichiometric IGP model are similar to those of the nonstoichiometric version, where the herbivore and omnivore both die of starvation. In general, increases in light intensity (K) could serve to stabilize the system, and when K was in the middle of its simulated range, increasing light intensity often allowed severely endangered

species to emerge again. In such cases, the herbivore and omnivore could coexist at any of the three states mentioned above (i.e. their populations could be constant, oscillatory, or irregular). For moderate to high values of light intensity, plant carrying capacity was determined by the availability of phosphorus P rather than by K , resulting in significant changes compared to the nonstoichiometric system. In contrast to that system, extremely high light intensity values in the stoichiometric system typically led to the omnivore becoming extinct earlier than the herbivore. Our finding that nutrient enrichment can reduce species diversity due to excessive predation is consistent with results in other ecological stoichiometric models (Boersma and Elser 2006; Peace et al. 2013, 2014). In summary, we found that too high or too low light intensity resulted in extinction of the herbivore and/or the omnivore, and that intermediate values of light intensity produced very rich model dynamics in which all three species could coexist in many different ways.

Our experiments also revealed patterns that emerged for different levels of nutrient availability P . Regardless of light intensity, coexistence of the three model species was impossible for low values of P , as expected given its necessity for growth. However, for light intensity values at which all model species could survive, the value taken for P affected whether chaos emerged, and if so, for which values of K it was present. As the amount of phosphorus available for use can vary from place to place, this finding means that changes in environmental phosphorus (such as nutrient loading in aquatic environments) can result in unpredictable population levels in ecosystems previously thought to be stable.

We found that under changing environmental conditions, both stoichiometric and nonstoichiometric IGP models can spend significant periods of time tracking steady states that are normally unstable. This means that the ability of a predator–prey system to track unstable states in a changing environment found in Arumugam et al. (2021) is robust to other forms of ecological interactions. We also found that the specific unstable steady state that the stoichiometric IGP model tracks can vary based on differences in initial conditions and rates of environmental change μ . Moreover, the tracking behaviour appears to last longer when the rate μ is faster. We can therefore conclude that even as the underlying conditions in an ecosystem change, IGP interspecies relationships have the ability to maintain their original dynamics for certain lengths of time. This is highly important for conservation, as it allows for a longer window of time than previously thought in which conservation measures can be put in place to reverse unfavourable environmental trends. However, due to the rich model behaviour that we found (including multistability) and the ability of our model to track several different unstable states depending on environmental conditions, the dynamics of an IGP community during this window could still be unpredictable. This necessitates further study on the behaviour of IGP systems in changing environments.

Our model involved two different kinds of ecological relationships, specifically predator–prey interactions and interspecific competition. We should point out that as three species are involved, this model is of relatively high dimensionality compared to others that have been previously studied. The complexity of the IGP model with a Holling type II functional response means that performing a complete mathematical analysis of the interior equilibria is quite difficult. Nevertheless, our model and its numerical results were still able to produce useful insights on species diversity and

conservation. In the future, mathematically, we will perform a rigorous analysis of the problems that we addressed numerically in this paper, and hence explore the full range of model dynamics. Biologically, we will incorporate stoichiometry into more ecological models and explore how it affects larger and more varied ecosystems, bringing even more constructive suggestions on how to protect species across many different functional groups.

Acknowledgements This research was partially supported by Natural Sciences and Engineering Research Council of Canada (Individual Discovery Grant RGPIN-2020-03911 and Discovery Accelerator Supplement Award RGPAS-2020-00090). We are grateful to the reviewers for their constructive and helpful comments.

Data Availability Data sharing is not applicable to this article as no datasets were generated or analyzed during the current study.

Declarations

Conflict of interest The authors declare that they have no conflict of interest.

Appendices

A. Proofs of stability results

A.1. Proof of Theorem 3.2

The Jacobian matrix of System (3.1) is

$$J = \begin{pmatrix} J_{11} & J_{12} & J_{13} \\ J_{21} & J_{22} & J_{23} \\ J_{31} & J_{32} & J_{33} \end{pmatrix},$$

where

$$\begin{aligned} J_{11} &= 1 - \frac{2u}{\min\{k, p - \beta_1 v - \beta_2 w\}} - \frac{v}{(1+u)^2} - \frac{\alpha_1 w}{(\alpha_1 + u)^2}, \\ J_{12} &= \begin{cases} -\frac{u}{1+u}, & k \leq p - \beta_1 v - \beta_2 w; \\ -\frac{\beta_1 u^2}{(p - \beta_1 v - \beta_2 w)^2} - \frac{u}{1+u}, & k > p - \beta_1 v - \beta_2 w. \end{cases} \\ J_{13} &= \begin{cases} -\frac{u}{\alpha_1 + u}, & k \leq p - \beta_1 v - \beta_2 w; \\ -\frac{\beta_2 u^2}{(p - \beta_1 v - \beta_2 w)^2} - \frac{u}{\alpha_1 + u}, & k > p - \beta_1 v - \beta_2 w. \end{cases} \\ J_{21} &= \begin{cases} \frac{\gamma_1 v}{(1+u)^2}, & \gamma_1 \beta_1 u \leq p - \beta_1 v - \beta_2 w; \\ -\frac{(p - \beta_1 v - \beta_2 w)v}{\beta_1(1+u)^2}, & \gamma_1 \beta_1 u > p - \beta_1 v - \beta_2 w. \end{cases} \end{aligned}$$

$$\begin{aligned}
 J_{22} &= \begin{cases} \frac{\gamma_1 u}{1+u} - \frac{\alpha_2 \varepsilon w}{(\alpha_2 + v)^2} - \delta_1, & \gamma_1 \beta_1 u \leq p - \beta_1 v - \beta_2 w; \\ \frac{p - 2\beta_1 v - \beta_2 w}{\beta_1(1+u)} - \frac{\alpha_2 \varepsilon w}{(\alpha_2 + v)^2} - \delta_1, & \gamma_1 \beta_1 u > p - \beta_1 v - \beta_2 w. \end{cases} \\
 J_{23} &= \begin{cases} -\frac{\varepsilon v}{\alpha_2 + v}, & \gamma_1 \beta_1 u \leq p - \beta_1 v - \beta_2 w; \\ -\frac{\beta_2 v}{\beta_1(1+u)} - \frac{\varepsilon v}{\alpha_2 + v}, & \gamma_1 \beta_1 u > p - \beta_1 v - \beta_2 w. \end{cases} \\
 J_{31} &= \begin{cases} \frac{\alpha_1 \gamma_2 w}{(\alpha_1 + u)^2}, & \gamma_2 \beta_2 u \leq p - \beta_1 v - \beta_2 w; \\ -\frac{(p - \beta_1 v - \beta_2 w)w}{\beta_2(\alpha_1 + u)^2}, & \gamma_2 \beta_2 u > p - \beta_1 v - \beta_2 w. \end{cases} \\
 J_{32} &= \begin{cases} \min \left\{ \gamma_3, \frac{\varepsilon \beta_1}{\beta_2} \right\} \frac{\alpha_2 w}{(\alpha_2 + v)^2}, & \gamma_2 \beta_2 u \leq p - \beta_1 v - \beta_2 w; \\ -\frac{\beta_1 w}{\beta_2(\alpha_1 + u)} + \min \left\{ \gamma_3, \frac{\varepsilon \beta_1}{\beta_2} \right\} \frac{\alpha_2 w}{(\alpha_2 + v)^2}, & \gamma_2 \beta_2 u > p - \beta_1 v - \beta_2 w. \end{cases} \\
 J_{33} &= \begin{cases} \frac{\gamma_2 u}{\alpha_1 + u} + \min \left\{ \gamma_3, \frac{\varepsilon \beta_1}{\beta_2} \right\} \frac{v}{\alpha_2 + v} - \delta_2, & \gamma_2 \beta_2 u \leq p - \beta_1 v - \beta_2 w; \\ \frac{p - \beta_1 v - 2\beta_2 w}{\beta_2(\alpha_1 + u)} + \min \left\{ \gamma_3, \frac{\varepsilon \beta_1}{\beta_2} \right\} \frac{v}{\alpha_2 + v} - \delta_2, & \gamma_2 \beta_2 u > p - \beta_1 v - \beta_2 w. \end{cases}
 \end{aligned}$$

At E_0 , the Jacobian matrix is

$$J(E_0) = \begin{pmatrix} 1 & 0 & 0 \\ 0 & -\delta_1 & 0 \\ 0 & 0 & -\delta_2 \end{pmatrix},$$

which has three eigenvalues: $\lambda_1 = 1 > 0$, $\lambda_2 = -\delta_1 < 0$ and $\lambda_3 = -\delta_2 < 0$. Thus E_0 is a saddle point with a two-dimensional stable manifold and is unstable.

At equilibrium E_1 , the Jacobian matrix is

$$J(E_1) = \begin{pmatrix} -1 & J_{12}^1 & J_{13}^1 \\ 0 & J_{22}^1 & 0 \\ 0 & 0 & J_{33}^1 \end{pmatrix}.$$

where

$$\begin{aligned}
 J_{22}^1 &= \begin{cases} \frac{\gamma_1 \bar{k}}{1 + \bar{k}} - \delta_1, & \gamma_1 \beta_1 \bar{k} \leq p; \\ \frac{p}{\beta_1(1 + \bar{k})} - \delta_1, & \gamma_1 \beta_1 \bar{k} > p, \end{cases} \\
 J_{33}^1 &= \begin{cases} \frac{\gamma_2 \bar{k}}{\alpha_1 + \bar{k}} - \delta_2, & \gamma_2 \beta_2 \bar{k} \leq p; \\ \frac{p}{\beta_2(\alpha_1 + \bar{k})} - \delta_2, & \gamma_2 \beta_2 \bar{k} > p. \end{cases}
 \end{aligned}$$

The eigenvalues of $J(E_1)$ are $\lambda_1 = -1$, $\lambda_2 = J_{22}^1$ and $\lambda_3 = J_{33}^1$. If

$$\max \left\{ \frac{\min \left\{ \gamma_1, \frac{p}{\beta_1 \bar{k}} \right\} \bar{k}}{\delta_1(1 + \bar{k})}, \frac{\min \left\{ \gamma_2, \frac{p}{\beta_2 \bar{k}} \right\} \bar{k}}{\delta_2(\alpha_1 + \bar{k})} \right\} < 1,$$

then λ_2 and $\lambda_3 < 0$. Thus E_1 is locally asymptotically stable. If

$$\max \left\{ \frac{\min \left\{ \gamma_1, \frac{p}{\beta_1 \bar{k}} \right\} \bar{k}}{\delta_1(1 + \bar{k})}, \frac{\min \left\{ \gamma_2, \frac{p}{\beta_2 \bar{k}} \right\} \bar{k}}{\delta_2(\alpha_1 + \bar{k})} \right\} > 1,$$

then λ_2 or $\lambda_3 > 0$, at least one eigenvalue is positive and hence E_1 is unstable (a saddle point).

A.2. Proof of Remark 3.3

Here, we show that E_1 is globally asymptotically stable. Define $L(t) = \sigma v(t) + w(t)$, where $\sigma = \frac{\gamma_3}{\varepsilon} + \frac{\beta_1}{\beta_2}$, and $\min \left\{ \gamma_3, \frac{\varepsilon \beta_1}{\beta_2} \right\} - \sigma \varepsilon < 0$. From the first equation of (3.1), we can obtain $u'(t) \leq u(1 - (u/\bar{k}))$. This yields that

$$\limsup_{t \rightarrow \infty} u(t) \leq \bar{k}.$$

Then for any $\eta > 0$, there exists $T > 0$ such that $u \leq \bar{k} + \eta$ for $t > T$. Note that

$$\begin{aligned} \frac{dL}{dt} &= \sigma \frac{dv}{dt} + \frac{dw}{dt} \\ &= \sigma v \left(\min \left\{ \gamma_1, \frac{p - \beta_1 v - \beta_2 w}{\beta_1 u} \right\} \frac{u}{1 + u} - \delta_1 \right) \\ &\quad + w \left(\min \left\{ \gamma_2, \frac{p - \beta_1 v - \beta_2 w}{\beta_2 u} \right\} \frac{u}{\alpha_1 + u} - \delta_2 \right) \\ &\quad + \left(\min \left\{ \gamma_3, \frac{\varepsilon \beta_1}{\beta_2} \right\} - \sigma \varepsilon \right) \frac{vw}{\alpha_2 + v} \\ &\leq \sigma v \left(\min \left\{ \gamma_1, \frac{p - \beta_1 v - \beta_2 w}{\beta_1 u} \right\} \frac{u}{1 + u} - \delta_1 \right) \\ &\quad + w \left(\min \left\{ \gamma_2, \frac{p - \beta_1 v - \beta_2 w}{\beta_2 u} \right\} \frac{u}{\alpha_1 + u} - \delta_2 \right) \\ &\leq \sigma v \left(\frac{\gamma_1 u}{1 + u} - \delta_1 \right) + w \left(\frac{\gamma_2}{\alpha_1 + u} - \delta_2 \right) \\ &\leq \sigma v \left(\frac{\gamma_1(\bar{k} + \eta)}{1 + \bar{k} + \eta} - \delta_1 \right) + w \left(\frac{\gamma_2(\bar{k} + \eta)}{\alpha_1 + \bar{k} + \eta} - \delta_2 \right) \end{aligned}$$

$$\begin{aligned} &\leq \max \left\{ \frac{\gamma_1(\bar{k} + \eta)}{1 + \bar{k} + \eta} - \delta_1, \frac{\gamma_2(\bar{k} + \eta)}{\alpha_1 + \bar{k} + \eta} - \delta_2 \right\} (\sigma v + w) \\ &= \max \left\{ \frac{\gamma_1(\bar{k} + \eta)}{1 + \bar{k} + \eta} - \delta_1, \frac{\gamma_2(\bar{k} + \eta)}{\alpha_1 + \bar{k} + \eta} - \delta_2 \right\} L. \end{aligned}$$

Since

$$\max \left\{ \frac{\gamma_1 \bar{k}}{\delta_1(1 + \bar{k})}, \frac{\gamma_2 \bar{k}}{\delta_2(\alpha_1 + \bar{k})} \right\} < 1,$$

for sufficiently small η , we have

$$\max \left\{ \frac{\gamma_1(\bar{k} + \eta)}{1 + \bar{k} + \eta} - \delta_1, \frac{\gamma_2(\bar{k} + \eta)}{\alpha_1 + \bar{k} + \eta} - \delta_2 \right\} < 0.$$

This implies that $\lim_{t \rightarrow \infty} L(t) = 0$, and hence $\lim_{t \rightarrow \infty} v(t) = \lim_{t \rightarrow \infty} w(t) = 0$. Furthermore, it follows from the fact that Ω is invariant that $\lim_{t \rightarrow \infty} u(t) = \bar{k}$. Therefore, $E_1 = (\bar{k}, 0, 0)$ is globally attractive. This, together with its local stability, proves that E_1 is globally asymptotically stable.

B. Proof of Theorem 3.5

An interior equilibrium $E^* = (u^*, v^*, w^*)$ of System (3.5) is a solution to the following three equations:

$$\left(1 - \frac{u}{k}\right) - \frac{v}{1 + u} - \frac{w}{\alpha_1 + u} = 0 \tag{B.1}$$

$$\frac{\gamma_1 u}{1 + u} - \frac{\varepsilon w}{\alpha_2 + v} - \delta_1 = 0, \tag{B.2}$$

$$\frac{\gamma_2 u}{\alpha_1 + u} + \frac{\gamma_3 v}{\alpha_2 + v} - \delta_2 = 0. \tag{B.3}$$

If $E^* = (u^*, v^*, w^*)$ is an interior equilibrium, from Eq. (B.3), we have

$$v^* = \frac{\alpha_2[\alpha_1 \delta_2 + (\delta_2 - \gamma_2)u^*]}{(\gamma_2 + \gamma_3 - \delta_2)u^* + \alpha_1(\gamma_3 - \delta_2)}.$$

Note that from the third equation (B.3), in order to have an interior equilibrium, another necessary condition is that

$$\gamma_2 + \gamma_3 - \delta_2 > \frac{\gamma_2 u}{\alpha_1 + u} + \frac{\gamma_3 v}{\alpha_2 + v} - \delta_2 = 0.$$

Moreover, v^* is positive provided that $u^* \in S_u$, where

$$S_u = \begin{cases} \left(\frac{\alpha_1(\delta_2 - \gamma_3)}{\gamma_2 + \gamma_3 - \delta_2}, \infty \right), & \max\{\gamma_2, \gamma_3\} < \delta_2 < \gamma_2 + \gamma_3, \\ (0, \infty), & \gamma_2 \leq \delta_2 \leq \gamma_3, \\ \left(\frac{\alpha_1(\delta_2 - \gamma_3)}{\gamma_2 + \gamma_3 - \delta_2}, \frac{\alpha_1\delta_2}{\gamma_2 - \delta_2} \right), & \gamma_3 < \delta_2 < \gamma_2, \\ \left(0, \frac{\alpha_1\delta_2}{\gamma_2 - \delta_2} \right), & \delta_2 < \min\{\gamma_2, \gamma_3\}. \end{cases}$$

From Eq. (B.1), we see it is necessary to require $u^* < k$. Substituting v^* into Eq. (B.2), we obtain

$$w^* = \frac{\alpha_2 + v^*}{\varepsilon} \left(\frac{\gamma_1 u^*}{1 + u^*} - \delta_1 \right).$$

To ensure $w^* > 0$, it is necessary that

$$u^* \in \left(\frac{\delta_1}{\gamma_1 - \delta_1}, k \right), \quad (\gamma_1 > \delta_1).$$

Eliminating v and w in Eq. (B.1), we obtain

$$\left(1 - \frac{u}{k} \right) (1 + u)[(\gamma_2 + \gamma_3 - \delta_2)u + \alpha_1(\gamma_3 - \delta_2)] = B_1 u + B_2,$$

where

$$B_1 = \alpha_1 \left[\frac{\gamma_3}{\varepsilon} (\gamma_1 - \delta_1) + (\delta_2 - \gamma_2) \right],$$

$$B_2 = \alpha_2 \left(\alpha_1 \delta_2 - \frac{\gamma_3 \delta_1}{\varepsilon} \right).$$

Let

$$D_1(u) = \left(1 - \frac{u}{k} \right) (1 + u)[(\gamma_2 + \gamma_3 - \delta_2)u + \alpha_1(\gamma_3 - \delta_2)]$$

and

$$D_2(u) = B_1 u + B_2.$$

If $\delta_2 < \gamma_3$, D_1 and D_2 has at most two intersections on the right side of the vertical axis.

Note that if $\delta_2 > \gamma_3$, D_1 and D_2 have at most three intersections on the right side of the vertical axis (see Fig. 26). Since $v^* \in S_v$, we must have $v^* > \frac{\alpha_1(\delta_2 - \gamma_3)}{\gamma_2 + \gamma_3 - \delta_2}$. Hence

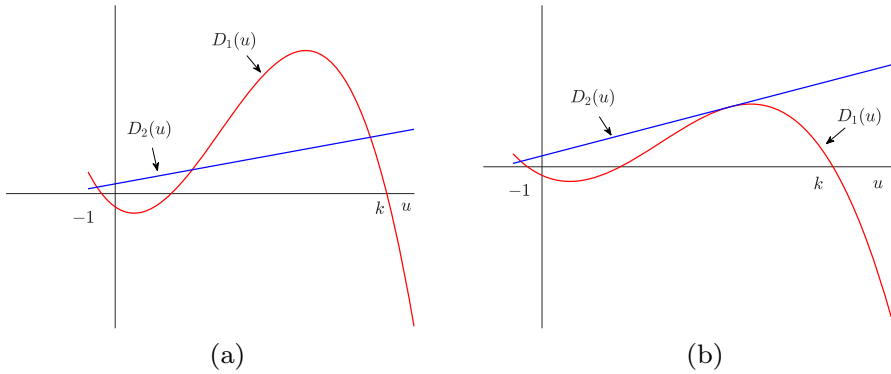


Fig. 26 $\delta_2 > \gamma_3$. Blue line: $D_2(u)$; Red curve: $D_1(u)$ (color figure online)

D_1 and D_2 have at most two intersections when $x^* \in \left(\frac{\alpha_1(\delta_2 - \gamma_3)}{\gamma_2 + \gamma_3 - \delta_2}, k\right)$. If $\gamma_1 > \delta_1$, $\gamma_2 + \gamma_3 > \delta_2$, and $S_E = S_u \cap \left(\frac{\delta_1}{\gamma_1 - \delta_1}, k\right) \neq \emptyset$, then System (3.5) has at most two interior equilibria, where $u_i^* \in S_E$ ($i = 1, 2$), $E^* \in \Omega^*$. Moreover, System (3.5) admits a saddle-node bifurcation when D_1 is tangent to D_2 .

C. Dynamics of interior equilibria

System (3.5) is a particular case of the stoichiometric system (3.1) in which the growth rate of the plant is limited by light availability and the growth rates of the herbivore and omnivore are both limited by carbon. Theorem 3.5 implies that the stoichiometric system (3.1) admits interior equilibria. Let $E^* = (u^*, v^*, w^*)$ be an interior equilibrium of System (3.1). Then, the Jacobian matrix at E^* reads as follows:

$$J(E^*) = \begin{pmatrix} J_{11}^* & J_{12}^* & J_{13}^* \\ J_{21}^* & J_{22}^* & J_{23}^* \\ J_{31}^* & J_{32}^* & J_{33}^* \end{pmatrix},$$

where

$$J_{11}^* = 1 - \frac{2u^*}{\min\{k, p - \beta_1 v^* - \beta_2 w^*\}} - \frac{v^*}{(1 + u^*)^2} - \frac{\alpha_1 w^*}{(\alpha_1 + u^*)^2},$$

$$J_{12}^* = \begin{cases} -\frac{u^*}{1 + u^*}, & k \leq p - \beta_1 v^* - \beta_2 w^*; \\ -\frac{\beta_1 (u^*)^2}{(p - \beta_1 v^* - \beta_2 w^*)^2} - \frac{u^*}{1 + u^*}, & k > p - \beta_1 v^* - \beta_2 w^*. \end{cases}$$

$$J_{13}^* = \begin{cases} -\frac{u^*}{\alpha_1 + u^*}, & k \leq p - \beta_1 v^* - \beta_2 w^*; \\ -\frac{\beta_2 (u^*)^2}{(p - \beta_1 v^* - \beta_2 w^*)^2} - \frac{u^*}{\alpha_1 + u^*}, & k > p - \beta_1 v^* - \beta_2 w^*. \end{cases}$$

$$\begin{aligned}
 J_{21}^* &= \begin{cases} \frac{\gamma_1 v^*}{(1+u^*)^2}, & \gamma_1 \beta_1 u^* \leq p - \beta_1 v^* - \beta_2 w^*; \\ -\frac{(p - \beta_1 v^* - \beta_2 w^*)v^*}{\beta_1(1+u^*)^2}, & \gamma_1 \beta_1 u^* > p - \beta_1 v^* - \beta_2 w^*. \end{cases} \\
 J_{22}^* &= \begin{cases} \frac{\gamma_1 u^*}{1+u^*} - \frac{\alpha_2 \varepsilon w^*}{(\alpha_2 + v^*)^2} - \delta_1, & \gamma_1 \beta_1 u^* \leq p - \beta_1 v^* - \beta_2 w^*; \\ \frac{p - 2\beta_1 v^* - \beta_2 w^*}{\beta_1(1+u^*)} - \frac{\alpha_2 \varepsilon w^*}{(\alpha_2 + v^*)^2} - \delta_1, & \gamma_1 \beta_1 u^* > p - \beta_1 v^* - \beta_2 w^*. \end{cases} \\
 J_{23}^* &= \begin{cases} -\frac{\varepsilon v^*}{\alpha_2 + v^*}, & \gamma_1 \beta_1 u^* \leq p - \beta_1 v^* - \beta_2 w^*; \\ -\frac{\beta_2 v^*}{\beta_1(1+u^*)} - \frac{\varepsilon v^*}{\alpha_2 + v^*}, & \gamma_1 \beta_1 u^* > p - \beta_1 v^* - \beta_2 w^*. \end{cases} \\
 J_{31}^* &= \begin{cases} \frac{\alpha_1 \gamma_2 w^*}{(\alpha_1 + u^*)^2}, & \gamma_2 \beta_2 u^* \leq p - \beta_1 v^* - \beta_2 w^*; \\ -\frac{(p - \beta_1 v^* - \beta_2 w^*)w^*}{\beta_2(\alpha_1 + u^*)^2}, & \gamma_2 \beta_2 u^* > p - \beta_1 v^* - \beta_2 w^*. \end{cases} \\
 J_{32}^* &= \begin{cases} \min \left\{ \gamma_3, \frac{\varepsilon \beta_1}{\beta_2} \right\} \frac{\alpha_2 w^*}{(\alpha_2 + v^*)^2}, & \gamma_2 \beta_2 u^* \leq p - \beta_1 v^* - \beta_2 w^*; \\ -\frac{\beta_1 w^*}{\beta_2(\alpha_1 + u^*)} + \min \left\{ \gamma_3, \frac{\varepsilon \beta_1}{\beta_2} \right\} \frac{\alpha_2 w^*}{(\alpha_2 + v^*)^2}, & \gamma_2 \beta_2 u^* > p - \beta_1 v^* - \beta_2 w^*. \end{cases} \\
 J_{33}^* &= \begin{cases} 0, & \gamma_2 \beta_2 u^* \leq p - \beta_1 v^* - \beta_2 w^*; \\ -\frac{w^*}{\alpha_1 + u^*}, & \gamma_2 \beta_2 u^* > p - \beta_1 v^* - \beta_2 w^*. \end{cases}
 \end{aligned}$$

Thus the characteristic equation of $J(E^*)$ is given by

$$\lambda^3 + p_1 \lambda^2 + p_2 \lambda + p_3 = 0,$$

where

$$\begin{aligned}
 p_1 &= -(J_{11}^* + J_{22}^* + J_{33}^*), \\
 p_2 &= J_{11}^* J_{22}^* + J_{11}^* J_{33}^* + J_{22}^* J_{33}^* - J_{12}^* J_{21}^* - J_{13}^* J_{31}^* - J_{23}^* J_{32}^*, \\
 p_3 &= J_{11}^* J_{23}^* J_{32}^* + J_{13}^* J_{22}^* J_{31}^* + J_{12}^* J_{21}^* J_{33}^* - J_{11}^* J_{22}^* J_{33}^* - J_{12}^* J_{23}^* J_{31}^* - J_{13}^* J_{32}^* J_{21}^*.
 \end{aligned}$$

From the Routh–Hurwitz criterion (Liu 1994), we know that E^* is locally asymptotically stable if $p_i > 0$ ($i=1,3$) and $p_1 p_2 - p_3 > 0$.

Remark C.1 Due to the complexity of System (3.1), we explore the dynamics of interior equilibria numerically. We take $r = 1.2; a_1 = 0.25; a_2 = 0.25; a_3 = 0.25; c_1 = 0.81; c_2 = 0.4; c_3 = 0.81; e_1 = 0.8; e_2 = 0.8; e_3 = 0.8; \theta_1 = 0.03; \theta_2 = 0.04; d_1 = 0.25; d_2 = 0.25; q = 0.0038; P = 0.04$, then the parameters of dimensionless system (3.1) are: $k = 4K, p = 42.1053, \gamma_1 = 0.54, \gamma_2 = 0.2667, \gamma_3 = 0.54, \alpha_1 = 1, \alpha_2 = 0.675, \beta_1 = 11.6959, \beta_2 = 31.5789, \delta_1 = 0.2083, \delta_2 = 0.2083, \varepsilon = 1.3669$. If we choose $K = 3.2$, that is $k = 12.8$, then System (3.1) has a unique interior equilibrium $E^* = (u^*, v^*, w^*) = (12.5854, 0.204, 0.0237)$. Notice

that $\gamma_1\beta_1u^* = 79.4867$, $\gamma_2\beta_2u^* = 105.9954$, $p - \beta_1v^* - \beta_2w^* = 38.9709$, then $p - \beta_1v^* - \beta_2w^* < \gamma_1\beta_1u^*$, $\gamma_2\beta_2u^*$. Hence we have

$$\begin{aligned}
 J_{11}^* &= 1 - \frac{2u^*}{k} - \frac{v^*}{(1+u^*)^2} - \frac{\alpha_1w^*}{(\alpha_1+u^*)^2} = -0.9677, \quad J_{12}^* = -\frac{u^*}{1+u^*} = 0.9264, \\
 J_{13}^* &= -\frac{u^*}{\alpha_1+u^*} = 0.9264, \\
 J_{21}^* &= -\frac{(p - \beta_1v^* - \beta_2w^*)v^*}{\beta_1(1+u^*)^2} = -0.00368, \quad J_{22}^* = \frac{p - 2\beta_1v^* - \beta_2w^*}{\beta_1(1+u^*)} \\
 &\quad - \frac{\alpha_2\varepsilon w^*}{(\alpha_2+v^*)^2} - \delta_1 = -0.0064, \\
 J_{23}^* &= -\frac{\beta_2v^*}{\beta_1(1+u^*)} - \frac{\varepsilon v^*}{\alpha_2+v^*} = -0.3578, \\
 J_{31}^* &= -\frac{(p - \beta_1v^* - \beta_2w^*)w^*}{\beta_2(\alpha_1+u^*)^2} = -0.00016, \\
 J_{32}^* &= -\frac{\beta_1w^*}{\beta_2(\alpha_1+u^*)} + \min\left\{\gamma_3, \frac{\varepsilon\beta_1}{\beta_2}\right\} \frac{\alpha_2w^*}{(\alpha_2+v^*)^2} = 0.00984, \\
 J_{33}^* &= -\frac{w^*}{\alpha_1+u^*} = -0.0017.
 \end{aligned}$$

Then we can obtain

$$\begin{aligned}
 p_1 &= -(J_{11}^* + J_{22}^* + J_{33}^*) = 0.9758 > 0, \\
 p_2 &= J_{11}^*J_{22}^* + J_{11}^*J_{33}^* + J_{22}^*J_{33}^* - J_{12}^*J_{21}^* - J_{13}^*J_{31}^* - J_{23}^*J_{32}^* = 0.0078 > 0, \\
 p_3 &= J_{11}^*J_{23}^*J_{32}^* + J_{13}^*J_{22}^*J_{31}^* + J_{12}^*J_{21}^*J_{33}^* - J_{11}^*J_{22}^*J_{33}^* - J_{12}^*J_{23}^*J_{31}^* - J_{13}^*J_{32}^*J_{21}^* \\
 &= 0.0034 > 0.
 \end{aligned}$$

Observe that $p_1p_2 - p_3 = 0.0042 > 0$, hence E^* is locally asymptotically stable. As shown in Fig. 10, the stoichiometric system therefore has a stable interior equilibrium when $K = 3.2$.

References

Andersen T (1997) Pelagic nutrient cycles: herbivores as sourced and sinks for nutrients. Springer, Berlin
 Andersen T, Hessen D (1991) Carbon, nitrogen, and phosphorus-content of fresh-water zooplankton. *Limnol Oceanogr* 36:807–814
 Andersen T, Elser J, Hessen D (2004) Stoichiometry and population dynamics. *Ecol Lett* 7:884–900
 Arumugam R, Lutscher F, Guichard F (2021) Tracking unstable states: ecosystem dynamics in a changing world. *Oikos* 130:525–540
 Attayde JL, van Nes EH, Araujo AIL et al (2010) Omnivory by planktivores stabilizes plankton dynamics, but may either promote or reduce algal biomass. *Ecosystems* 13:410–420
 Boersma M, Elser JJ (2006) Too much of a good thing: on stoichiometrically balanced diets and maximal growth. *Ecology* 87:1325–1330
 Chen M, Fan M, Kuang Y (2017) Global dynamics in a stoichiometric food chain model with two limiting nutrients. *Math Biosci* 289:9–19

- Chen M, Fan M, Xie C, Peace A, Wang H (2018) Stoichiometric food chain model on discrete time scale. *Math Biosci Eng* 16:101–118
- Crous KY, Quentin AG, Lin Y-S, Medlyn BE, Williams DG, Barton CVM, Ellsworth DS (2013) Photosynthesis of temperate Eucalyptus globulus trees outside their native range has limited adjustment to elevated CO₂ and climate warming. *Glob Change Biol* 19:3790–3807
- Duarte CM (1992) Nutrient concentration of aquatic plants: patterns across species. *Limnol Oceanogr* 37:882–889
- Dusenge ME, Duarte AG, Way DA (2019) Plant carbon metabolism and climate change: elevated CO₂ and temperature impacts on photosynthesis, photorespiration and respiration. *New Phytol* 221:32–49
- Elser JJ, Dobberfuhl D, MacKay NA, Schampel JH (1996) Organism size, life history, and N: P stoichiometry: towards a unified view of cellular and ecosystem processes. *Bioscience* 46:674–684
- Fedriani JM, Fuller TK, Sauvajot RM, York EC (2000) Competition and intraguild predation among three sympatric carnivores. *Oecologia* 125:258–270
- Gerber GP, Echternacht AC (2000) Evidence for asymmetrical intraguild predation between native and introduced Anolis lizards. *Oecologia* 124:599–607
- Glibert PM (2012) Ecological stoichiometry and its implications for aquatic ecosystem sustainability. *Curr Opin Environ Sustain* 4:272–277
- Han R, Dai B, Wang L (2018) Delay induced spatiotemporal patterns in a diffusive intraguild predation model with Beddington–DeAngelis functional response. *Math Biosci Eng* 15:595–627
- Heggerud CM, Wang H, Lewis MA (2020) Transient dynamics of a stoichiometric cyanobacteria model via multiple-scale analysis. *SIAM J Appl Math* 80:1223–1246
- Holling CS (1959a) The components of predation as revealed by a study of small-mammal predation of the European pine sawfly. *Can Entomol* 91:293–320
- Holling CS (1959b) Some characteristics of simple types of predation and parasitism. *Can Entomol* 91:385–398
- Holling CS (1966) The functional response of invertebrate predators to prey density. *Mem Entomol Soc Can* 98:5–86
- Holt RD, Polis GA (1997) A theoretical framework for intraguild predation. *Am Nat* 149:745–764
- Hsu S-B, Ruan S, Yang T-H (2015) Analysis of three species Lotka–Volterra food web models with omnivory. *J Math Anal Appl* 426:659–687
- Jeyasingh PD, Goos JM, Thompson SK, Godwin CM, Cotner JB (2017) Ecological stoichiometry beyond redfield: an ionic perspective on elemental homeostasis. *Front Microbiol* 8:722
- Ji J, Wang L (2022) Competitive exclusion and coexistence in an intraguild predation model with Beddington–DeAngelis functional response. *Commun Nonlinear Sci Numer Simul* 107:106192
- Ji J, Lin G, Wang L (2022a) Effects of intraguild prey dispersal driven by intraguild predator-avoidance on species coexistence. *Appl Math Model* 103:51–67
- Ji J, Lin G, Wang L, Mai A (2022b) Spatiotemporal dynamics induced by intraguild predator diffusion in an intraguild predation model. *J Math Biol* 85:1–28
- Kuang Y, Huisman J, Elser JJ (2004) Stoichiometric plant-herbivore models and their interpretation. *Math Biosci Eng* 1:215–222
- Leung M, Padilla D, Song B, Kang Y, Shemer N, Vinagera J (2015) A symmetric intraguild predation model for the invasive lionfish and native grouper. *Commun Math Biol Neurosci* 2015
- Li X, Wang H (2010) A stoichiometrically derived algal growth model and its global analysis. *Math Biosci Eng* 7:825–836
- Li X, Wang H, Kuang Y (2011) Global analysis of a stoichiometric producer-grazer model with Holling type functional responses. *J Math Biol* 63:901–932
- Lin L, Peckham B, Stech H, Pastor J (2012) Enrichment in a stoichiometric model of two producers and one consumer. *J Biol Dyn* 6:97–116
- Liu WM (1994) Criterion of Hopf bifurcations without using eigenvalues. *J Math Anal Appl* 182:250–256
- Loladze I, Kuang Y, Elser JJ (2000) Stoichiometry in producer-grazer systems: linking energy flow with element cycling. *Bull Math Biol* 62:1137–1162
- Loladze I, Kuang Y, Elser J, Fagan W (2004) Competition and stoichiometry: coexistence of two predators on one prey. *Theor Popul Biol* 65:1–15
- Lonsinger RC, Gese EM, Bailey LL, Waits LP (2017) The roles of habitat and intraguild predation by coyotes on the spatial dynamics of kit foxes. *Ecosphere* 8:e01749
- Moe SJ, Stelzer RS, Forman MR, Harpole WS, Daufresne T, Yoshida T (2005) Recent advances in ecological stoichiometry: insights for population and community ecology. *Oikos* 109:29–39

- Moore JK, Doney SC, Kleypas JA, Glover DM, Fung IY (2002) An intermediate complexity marine ecosystem model for the global domain. *Deep Sea Res Part II*(49):403–462
- Mumby PJ, Harborne AR, Brumbaugh DR (2011) Grouper as a natural biocontrol of invasive lionfish. *PLoS ONE* 6:e21510
- Peace A (2015) Effects of light, nutrients, and food chain length on trophic efficiencies in simple stoichiometric aquatic food chain models. *Ecol Modell* 312:125–135
- Peace A, Zhao Y, Loladze I, Elser JJ, Kuang Y (2013) A stoichiometric producer-grazer model incorporating the effects of excess food-nutrient content on consumer dynamics. *Math Biosci* 244:107–115
- Peace A, Wang H, Kuang Y (2014) Dynamics of a producer-grazer model incorporating the effects of excess food nutrient content on grazers growth. *Bull Math Biol* 76:2175–2197
- Pilati A, Vanni MJ (2007) Ontogeny, diet shifts, and nutrient stoichiometry in fish. *Oikos* 116:1663–1674
- Redfield AC (1958) The biological control of chemical factors in the environment. *Am Sci* 46:205–221
- Robakowski P, Li Y, Reich PB (2012) Local ecotypic and species range-related adaptation influence photosynthetic temperature optima in deciduous broadleaved trees. *Plant Ecol* 213:113–125
- Rong X, Sun Y, Fan M, Wang H (2020) Stoichiometric modeling of Aboveground–Belowground interaction of herbaceous plant and two herbivores. *Bull Math Biol* 82:107
- Scheffer M, Rinaldi S, Kuznetsov YA, van Nes EH (1997) Seasonal dynamics of *Daphnia* and algae explained as a periodically forced predator–prey system. *Oikos* 80:519–532
- Sen D, Ghorai S, Banerjee M (2018) Complex dynamics of a three species prey–predator model with intraguild predation. *Ecol Complex* 34:9–22
- Shu H, Hu X, Wang L, Watmough J (2015) Delay induced stability switch, multi-type bistability and chaos in an intraguild predation model. *J Math Biol* 71:1269–1298
- Sterner RW, Elser JJ (2002) *Ecological stoichiometry*. Princeton University, Princeton
- Wang H, Smith HL, Kuang Y, Elser JJ (2007) Dynamics of stoichiometric bacteria–algae interactions in the epilimnion. *SIAM J Appl Math* 68:503–522
- Xie T, Yang X, Li X, Wang H (2018) Complete global and bifurcation analysis of a stoichiometric predator–prey model. *J Dyn Differ Equ* 30:447–472

Publisher's Note Springer Nature remains neutral with regard to jurisdictional claims in published maps and institutional affiliations.

Springer Nature or its licensor (e.g. a society or other partner) holds exclusive rights to this article under a publishing agreement with the author(s) or other rightsholder(s); author self-archiving of the accepted manuscript version of this article is solely governed by the terms of such publishing agreement and applicable law.